NASA CR180879

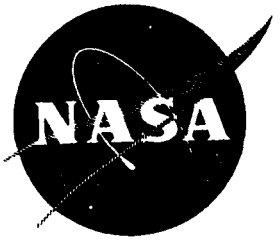

SPACECRAFT DIELECTRIC SURFACE CHARGING PROPERTY DETERMINATION

by W.S. Williamson

HUGHES RESEARCH LABORATORIES

prepared for

NATIONAL AERONAUTICS AND SPACE ADMINISTRATION

NASA Lewis Research Center
Contract NAS 3-22540

1. Report No.	2. Government Accession No.	3. Recipient's Catalog No.
CR180879		

4. Title and Subtitle	5. Report Date
SPACECRAFT DIELECTRIC CHARGING PROPERTY DETERMINATION	October 1987
	6. Performing Organization Code

7. Author(s)	8. Performing Organization Report No.
W.S. Williamson	
	10. Work Unit No. 506-55-72

9. Performing Organization Name and Address	11. Contract or Grant No.
Hughes Research Laboratories 3011 Malibu Canyon Road Malibu, CA 90265	NAS 3-22540
	13. Type of Report and Period Covered Final Sept. 1980 to Nov. 1981

12. Sponsoring Agency Name and Address	14. Sponsoring Agency Code
NASA Lewis Research Center 21000 Brookpark Road Cleveland, OH 44135	

15. Supplementary Notes

16. Abstract

The charging properites of 127-μm-thick polyimide, (a commonly used spacecraft dielectric material) have been measured under conditions of irradiation by a low-current-density (3-μAm^{-2}) electron beam with energy between 2 keV and 14 keV. The observed charging characteristics were consistent with predictions of the NASCAP computer model. The use of low electron current density results in a nonlinearity in the sample-potential versus beam-energy characteristic which is attributed to conduction leakage through the sample. Microdischarges were present at relatively low beam energies.

17. Key Words (Suggested by Author(s))	18. Distribution Statement
Spacecraft charging Dielectrics NASCAP Computer Modeling	Unclassified Publicly Available

19. Security Classif. (of this report)	20. Security Classif. (of this page)	21. No. of pages	22. Price*
Unclassified	Unclassified	80	

*For sale by the National Technical Information Service, Springfield, Virginia 22161

TABLE OF CONTENTS

LIST OF ILLUSTRATIONS AND TABLES

LIST OF ILLUSTRATIONS AND TABLES (continued)

LIST OF ILLUSTRATIONS AND TABLES (continued)

ACKNOWLEDGMENT

The Plasma Physics Department staff gratefully acknowledges the assistance of Bill Elkman of Hughes Space and Communications group, who conducted the NASCAP computer runs. His work was supported by Hughes IR&D funds.

SECTION 1

INTRODUCTION

In the early seventies, several geosynchronous satellites began experiencing a series of electronic switching anomalies.[1] These events occurred predominantly in the local midnight-to-dawn quadrant of the orbit. The anomalies were generally in the nuisance category, not detrimental to satellite performance and were usually corrected, catalogued, and forgotten. However, the occurrence of a complete power failure of a synchronous satellite in June 1973 indicated a problem of major proportions. The failure could have been caused by an encounter with a severe geomagnetic substorm.[1] These substorms have been known to occur at various times, as evidenced by both ground observations and ATS-5 flight data.[2-4] The ATS-5 data, supported by more recent ATS-6 data,[5,6] have shown that plasma clouds of relatively high energies (1 to 50 keV) were injected into geosynchronous regions at local midnight. Satellites encountering these clouds could have had their surfaces charged to significant negative voltages.[4] If a voltage threshold were exceeded, then discharges could occur and the resultant transient could couple into the low-level command logic systems being used and be interpreted as a command - triggering the anomaly.

The realization that the geosynchronous environment could cause surface charging and induce satellite electronic system anomalies resulted in the establishment of a cooperative AF/NASA Spacecraft Charging Technology Investigation.[7] The goal of this investigation is to establish design criteria to control detrimental effects that result from surface charging by the geosynchronous environment. The approach used to evaluate these charging phenomena was to establish a computer code capable of predicting surface charging on a variety of sample configurations in both ground simulation facilities and space environments. This code, called the NASA Charging Analyzer Program, or NASCAP,[8,9]

would be validated against ground test results and the Spacecraft Charging At The High Altitudes (SCATHA) satellite flight data.[10] Based on this validation, the code was to be used as the means of evaluating designs of the more complex satellites planned for future missions.

Since the NASCAP code validation depended on limited ground test results and one set of satellite data, and the code is to be used as the principal means of extrapolating surface charging effects on future spacecraft, it is vital to demonstrate that the code could predict accurate results under all possible conditions. Ground tests on samples ranging from single dielectrics to complex objects with many materials have been conducted to provide a data base.[11,12] Total- and secondary-yield measurements of dielectrics have been made[13] and a detailed evaluation of SCATHA data was undertaken.[10,14] All these results were compared to NASCAP predictions to validate the physics of the code and verify its predictive capabilities. The agreement was excellent.

As part of this validation and verification procedure, a contractual program was initiated at Hughes Research Laboratories (HRL) to test Kapton polyimide samples under various conditions and to compare the results to NASCAP predictions. The available capabilities of the HRL facilities were to be used for comparisons under conditions not available elsewhere. Kapton was chosen as the test material since it is used on large areas of most spacecraft. The iterative procedure envisioned for obtaining the best estimate of the material properties is illustrated in Figure 1.

The experiment plan called for testing under irradiation by monoenergetic electrons (with particle energies in the range of 1 to 14 keV) or ions (with particle energies between 5 and 10 keV), either in vacuum-ultraviolet illumination or dark conditions, and at various incident current densities. The sample was to be exposed to normally incident beams and beams at various non-normal angles of incidence. The data output would be the

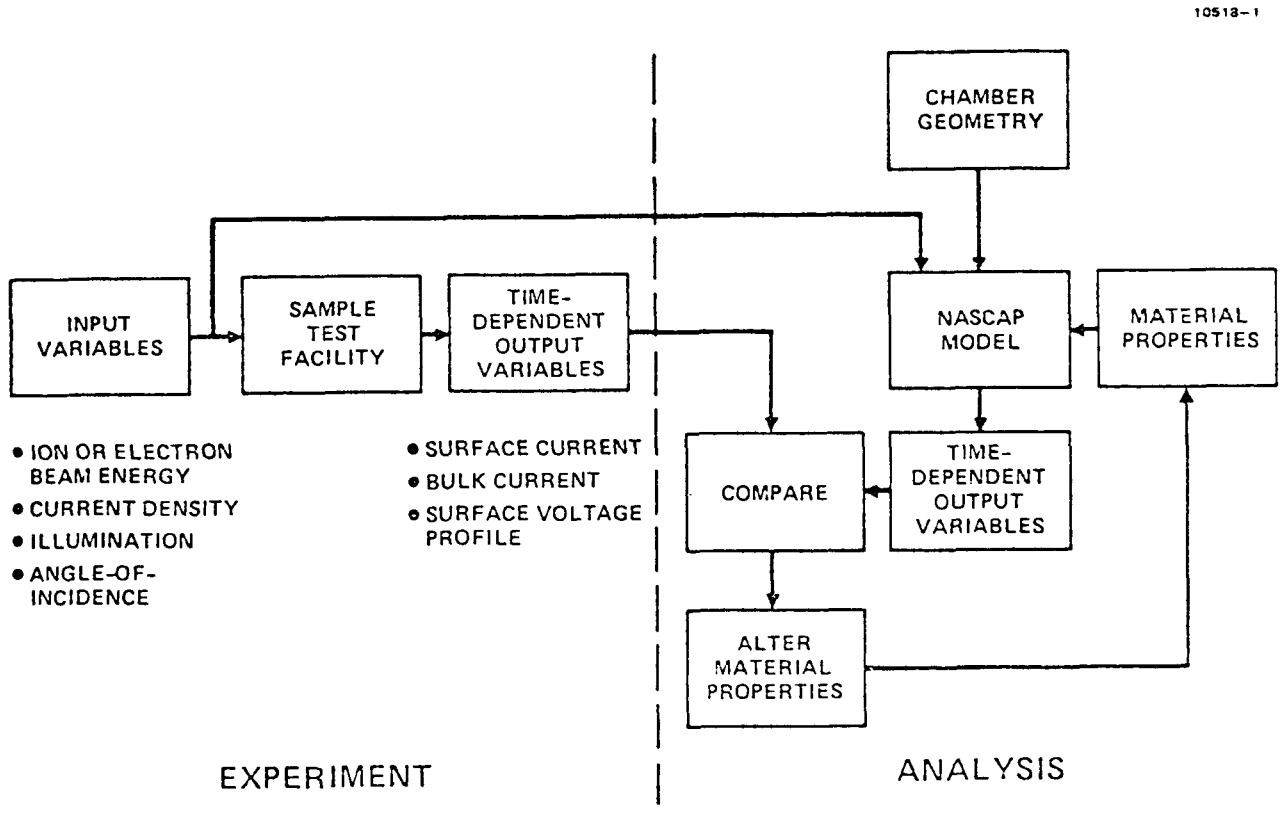

Figure 1. Procedure for calculating material-property values.

leakage current and surface voltage profile as functions of charging time. The analysis would start with the simplified one-dimensional model in NASCAP (the Materials Charging or Matching routine) for a preliminary comparison between prediction and experiment. Properties used by the code would be adjusted as required to improve the comparison. Then the full NASCAP code would be used for the final comparison and adjustment of material properties as required. Since NASCAP would predict electric fields in space as a function of given sample charging conditions, the influence of chamber size on charging characteristics could also be evaluated.

Unfortunately, the complete program of testing and comparisons was not completed due to unanticipated difficulties. Only the experiments with normal-incidence electrons and with the sample in the dark were completed. The work that was accomplished is detailed in Section 2, Experimental Investigation, and in Section 3, Analytical Investigation. A discussion of the results and recommendations for future work is given in Section 4.

SECTION 2

EXPERIMENTAL INVESTIGATION

2.1 FACILITY DESCRIPTION

2.1.1 Overview

The tests for this investigation were conducted in the HRL spacecraft charging simulation facility shown schematically in Figure 2. This facility consists of a main vacuum chamber and a smaller test-section chamber.[15] The main chamber (0.61-m diameter by 1.87-m long) is oil-diffusion pumped and is capable of maintaining a pressure between 10^{-4} and 10^{-5} Pa (10^{-6} to 10^{-7} Torr). The environmental simulation devices – electron flood gun, ion gun, and UV source – are located in this chamber. Because of chamber constraints at the time this study was done, only the electron gun or the ion gun could be installed at any one time.

The sample being evaluated is located in the smaller antechamber (0.29-m in diameter by 0.4-m long). This chamber can be isolated from the main chamber with a gate valve. The details of this chamber are shown in Figure 3.

2.1.2 Environment Simulation Devices

The electron and ion sources that we employed in this program are simple devices employing dc electrostatic acceleration of electrons emitted from a hot thermionic cathode, and ions formed in a Penning discharge, respectively. Both particle sources are based on proven designs, and they have afforded reliable performance for this program. The electron source design is essentially identical to a NASA-LeRC-developed source used extensively in testing. The ion source is a modification of the design used in the Hughes-developed Satellite Positive Ion Beam Source (SPIBS) experiment flown successfully on the SCATHA satellite.

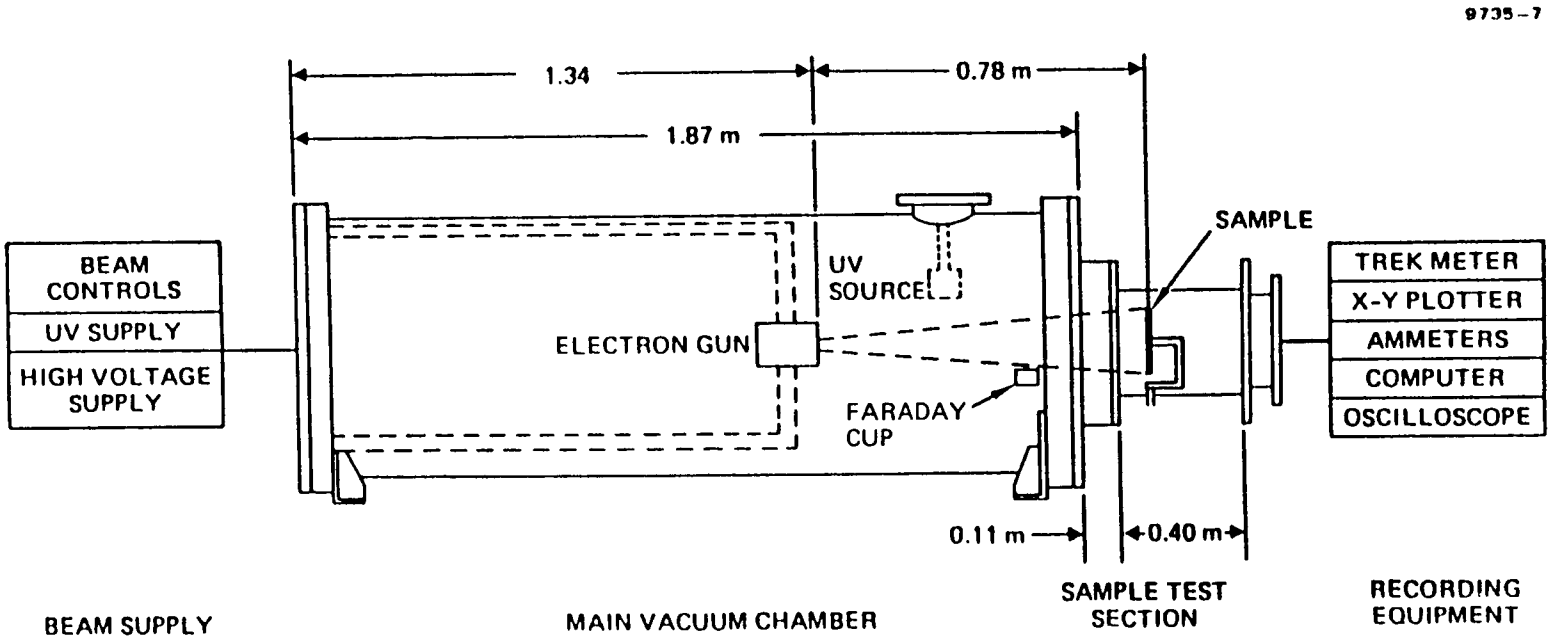

Figure 2. Hughes spacecraft-charging-simulation facility: Overview.

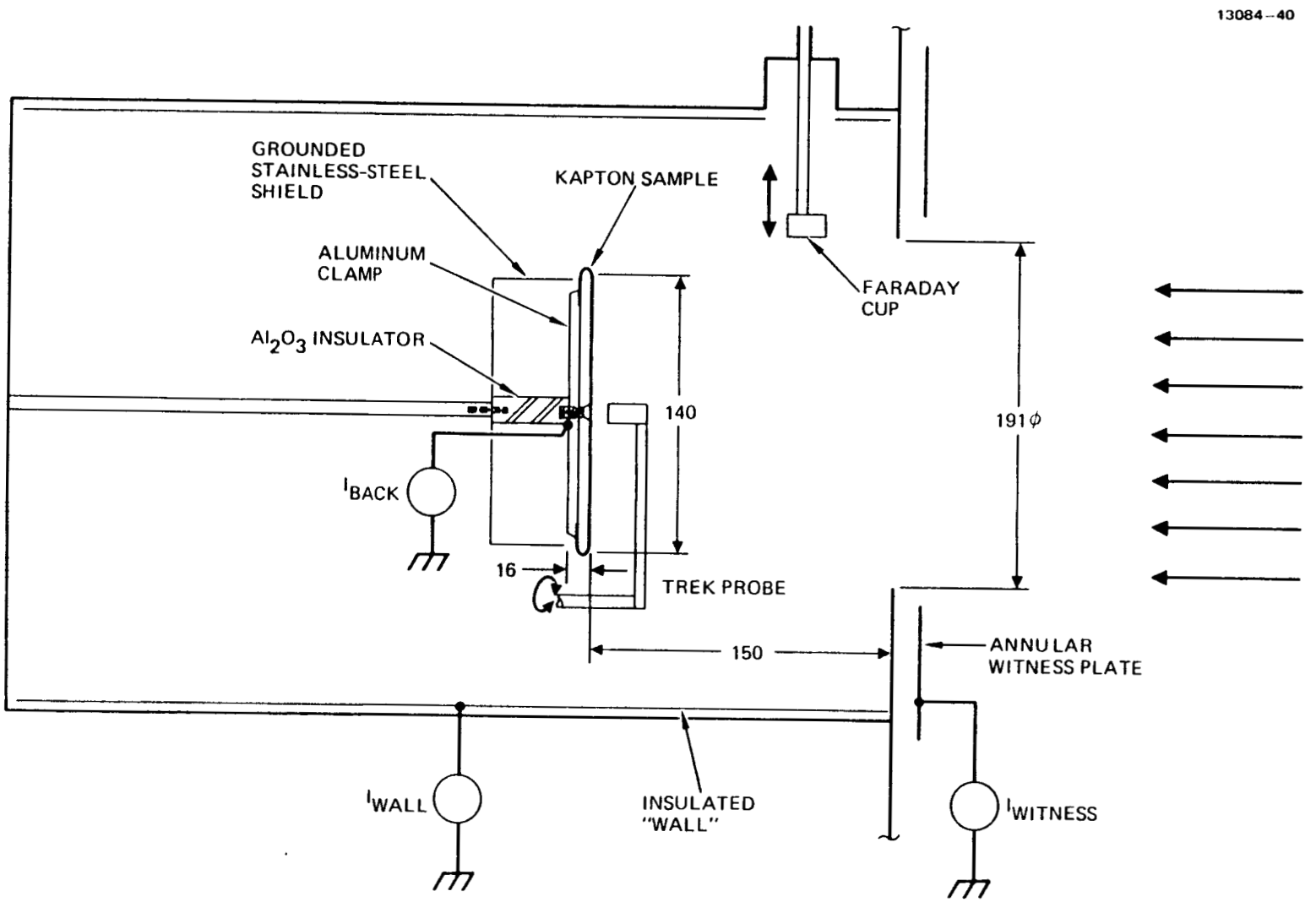

Figure 3. Hughes spacecraft-charging-simulation facility: sample test section details.

2.1.2.1 Electron Flood Gun

Description

The electron source is illustrated schematically in Figure 4. It consists of a filamentary cathode which is located at the center of curvature of three wire-mesh grids which serve as the extraction electrodes. The first two grids (nos. 1 and 2, nearest the filament) are connected together and biased slightly positive with respect to the filament. These grids serve to extract electrons from the filament with a small (100-V) potential difference. The large potential difference that is associated with the beam energy is maintained between the second and third grids. The filament/first-grid region is shielded from this large electric field by the large equipotential space that is present between the second and third grids. Electrons that emerge from the second grid are accelerated to final energy in the gap formed by grid Nos. 2 and 3. This gap has the shape of a section of a spherical shell. Because the rapid divergence of the beam produces a scale length that is many times that of the optics, the beam possesses a high degree of spatial uniformity.

Another feature of this electron-source design is that the filament is housed in a cylindrical cathode tube that is fitted with an annular end cap. The presence of this end cap has two beneficial results. First, electrons emitted from the filament must pass through a well-defined restrictive aperture before receiving much acceleration, so that the current-density distribution is largely independent of filament geometry. Second, the end cap prevents light from the filament from directly reaching the sample. This is an important electron-source characteristic when photosensitive materials, such as Kapton, are being tested.

Calibration

Electron beam current density profiles were recorded for each specified beam voltage using a grounded copper calibration sample. The beam current density as a function of the transverse

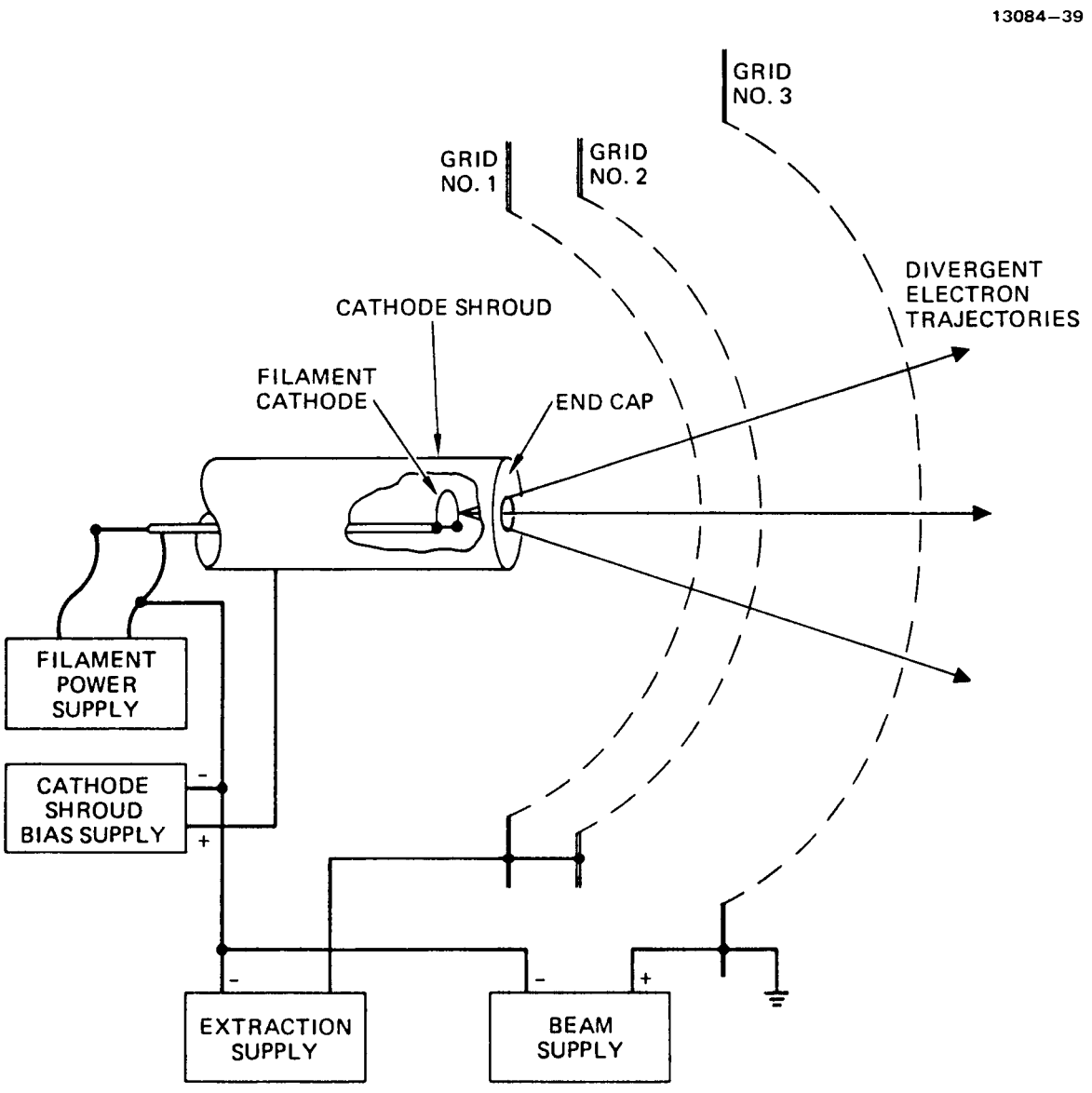

Figure 4. Electron source (NASA LeRC Design).

coordinate (x-axis) at the center of this grounded calibration plate was obtained with a Faraday cup located 90 mm in front of the sample. The grounded sample provided a uniform potential surface that would not cause the beam to diverge. The Faraday cup collector was biased to +45 V to suppress secondaries. Typical results of these measurements are shown in Figures 5 and 6. As can be seen from these measurements, the beam is fairly uniform in the range of accelerating potentials between 4 and 10 kV. Outside this range of values there is a slight skewness.

Figure 7 shows the current density profiles for various beam voltages with the Kapton target in place. A definite "hot spot" existed in the 4-kV beam voltage case. Otherwise, the characteristics are similar to those obtained in the grounded sample tests.

The calibration curves tend to be reproducible during a given day and do change with filament age. The "hot spot" noted above disappeared when filaments were changed.

An attempt was made to increase beam uniformity and alignment with the sample center by means of electrostatic deflection plates. This was unsuccessful because beam focusing and beam pointing could not be controlled independently. Magnetic deflection would probably be more successful.

2.1.2.2 Proton Flood Gun

Description

The ion source is shown schematically in Figure 8. It consists of a small Penning discharge chamber with a filamentary cathode and an anode guarded by the magnetic field that is produced by several axial permanent magnets and iron pole pieces at each end of the discharge chamber. Hydrogen gas (or other gases, as desired) is admitted through the upstream endplate of the source and ionized in the discharge. Ions are extracted through a single, small aperture located centrally on the downstream discharge-chamber endplate. The three-grid extraction

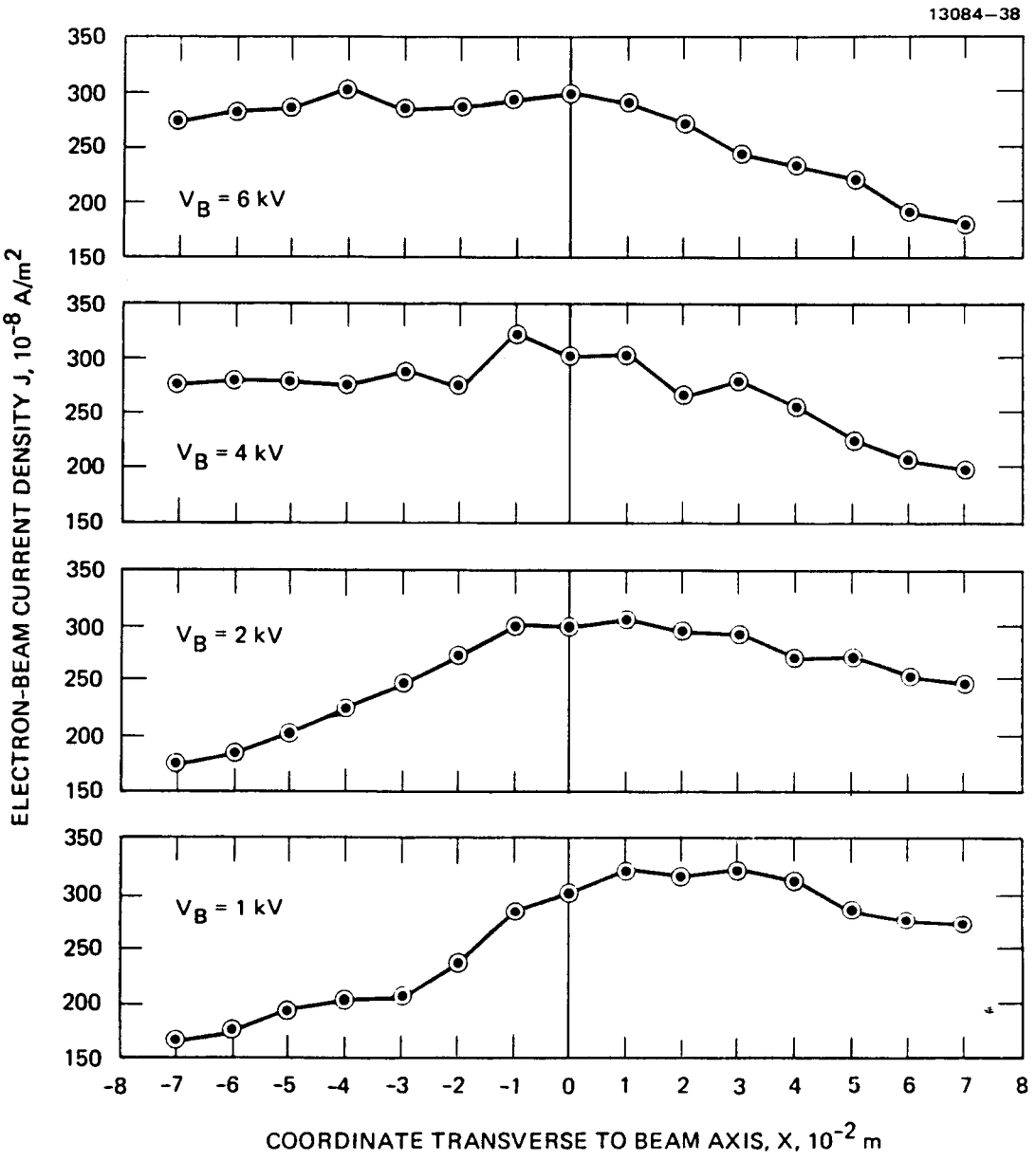

Figure 5. Electron-beam-current density profiles for copper target: values for 1 kV $< V_B <$ 6 kV.

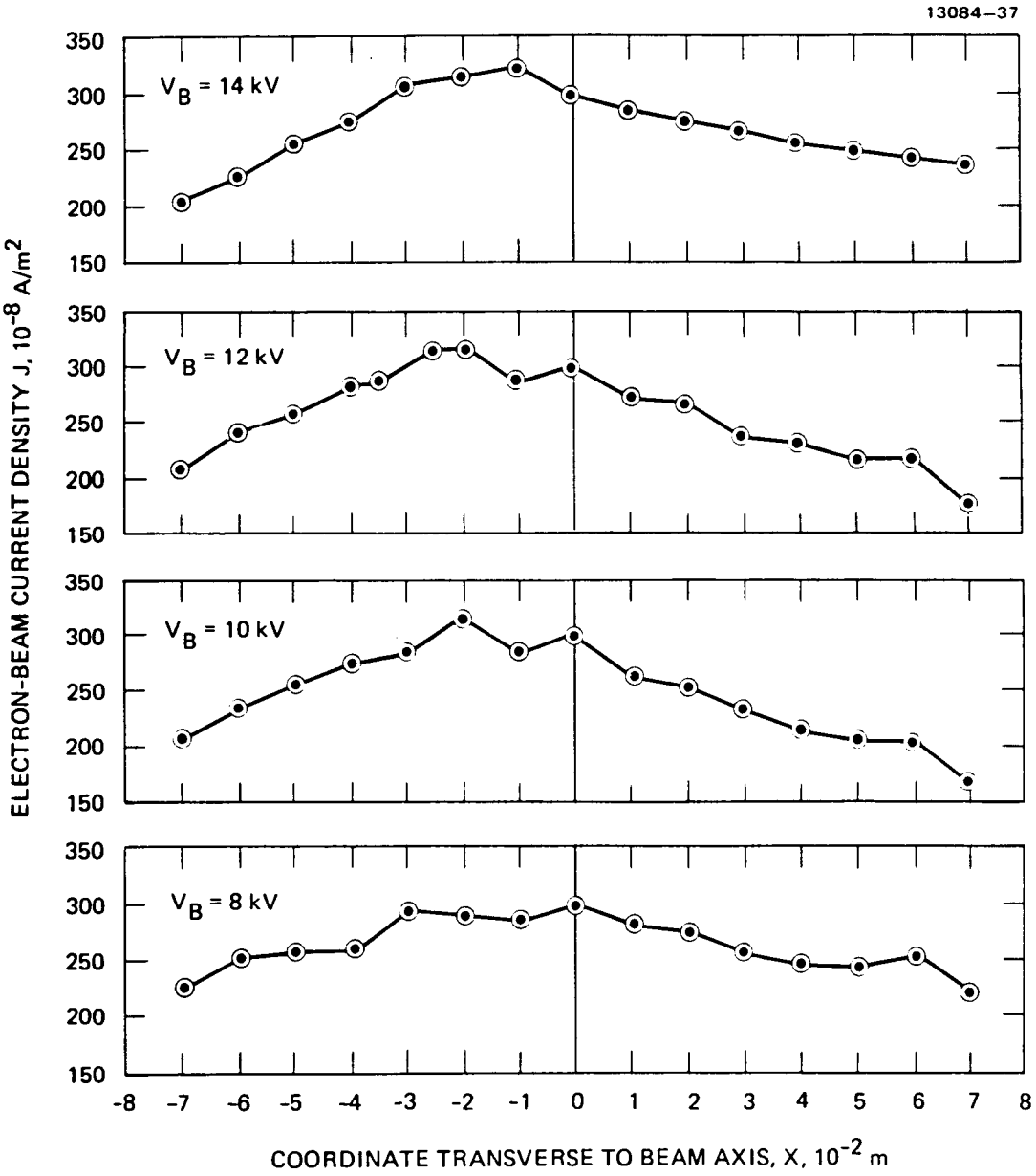

Figure 6. Electron-beam-current density profiles for copper target: values for 8 kV $<V_B<$ 14 kV.

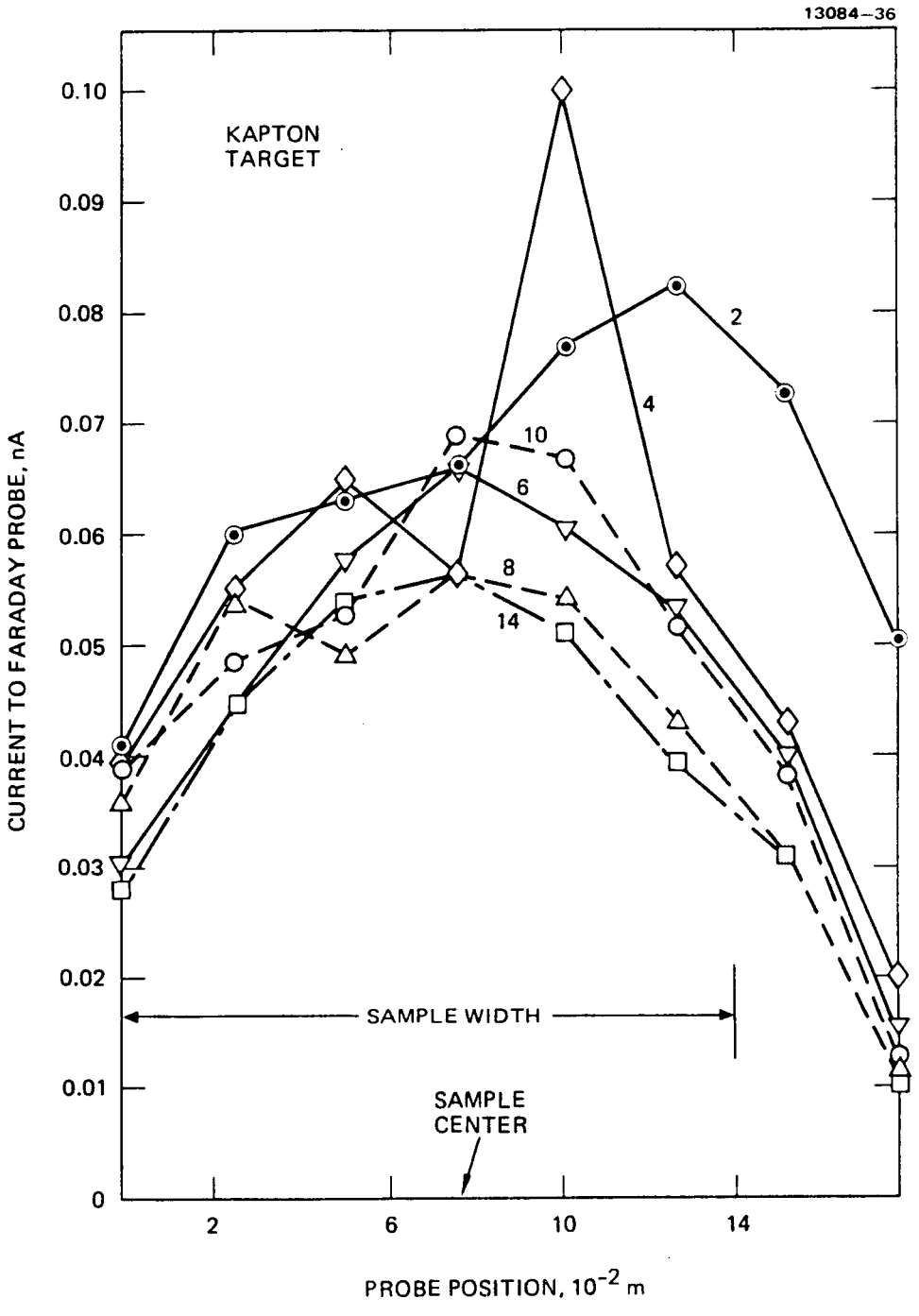

Figure 7. Electron-beam-current density profiles. Kapton target.

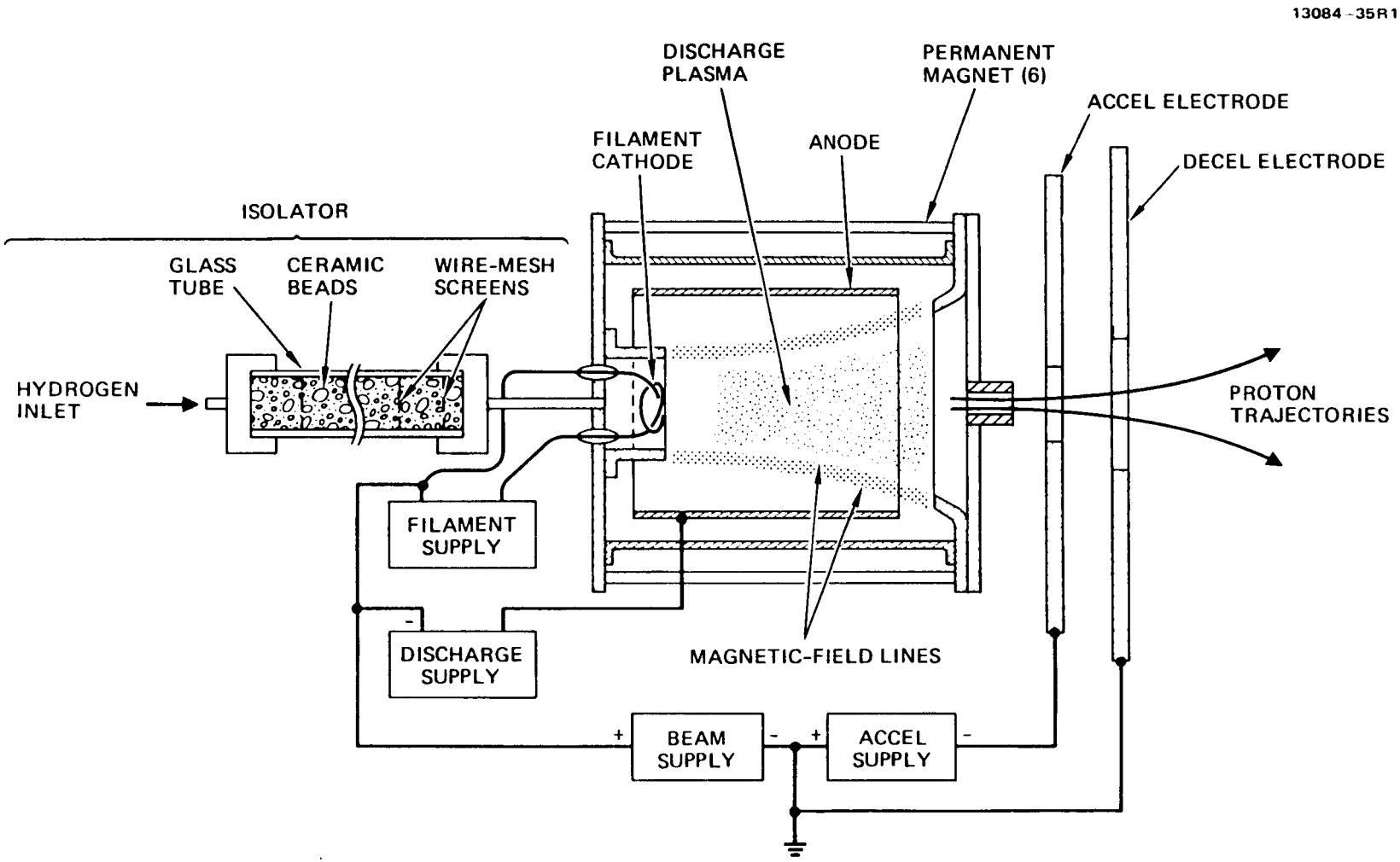

Figure 8. Ion source, showing single aperture optics. The proton beam exits with an energy corresponding to the sum of the voltages of the beam and discharge power supplies.

system is designed to produce a large degree of divergence in the ion beam. The furthest upstream grid (the discharge-chamber endplate) is maintained at the full beam voltage (up to 15 kV), the second grid is negative with respect to ground, and the third grid is grounded. Gas being supplied to the discharge chamber passes through a long glass tube filled with ceramic beads and wire-mesh spacers. This high-voltage isolating structure, which ensures that the hydrogen gas does not undergo Paschen breakdown, presently limits the available beam energy to 15 keV; this limit could easily be raised by increasing the isolator length.

This ion source is essentially the same as that used on the SPIBS experiment, which was used to study spacecraft-charging phenomena by ejecting a positive xenon-ion beam. The SPIBS beam could be ejected either with or without space-charge neutralization from a filamentary electron emitter that was located just downstream of the third grid. We modified this ion source for the present application by replacing the ion-beam-extraction system with a single-aperture, divergent-beam type, replacing the hollow cathode with a filamentary thermionic cathode, and adding a longer isolator consistent with the higher voltages required.

Calibration

The proton source was operated in a large glass-cross vacuum system to determine its characteristics. It was found that the beam exhibited a divergence angle of approximately 30 degrees. The proton current density was measured at a 10-cm distance. Extrapolation of these data to the 2-m separation in the environmental simulation facility indicated that proton current densities between 0.0 and 200 pA/cm^2 would be available. The source operated stably and reproducibly over the beam energy range of 0.0 to 15 keV, and its operation produced only a minimal gas loading on the vacuum facility.

2.1.2.3 Ultraviolet Source

Description

The ultraviolet source used in this facility is a krypton source manufactured by Quantatec (Model 398). It is mounted off-axis and uses a magnesium-fluoride mirror to reflect the beam onto the sample (the mirror is not shown in Figure 2).

Calibration

This system was calibrated in the chamber to ensure that the sample would receive the equivalent of one sun ultraviolet irradiation.

2.1.3 Test Samples

Standard 127-μm (5-mil) thick aluminumized Kapton material was used for the test surfaces. A square area of Kapton, 141 mm on a side (total area of 0.02 m^2), was exposed to the beam.

The Kapton was mounted with the aluminum surface against the metal mounting plate. The edges of the aluminumized Kapton were wrapped around the ends of the mounting plate and clamped in position with an aluminum support plate (see Figure 3). No adhesives were used. The clamping plate was mounted to a vertical shaft through an alumina insulator. A grounded stainless steel shield was used to prevent scattered-electron collection on the back of the sample. The whole assembly could be rotated to vary the angle of incidence between the beam and the sample surface.

2.1.4 Instrumentation

2.1.4.1 Surface Voltage Measurements

Sample surface voltage measurements were made without interrupting the beam charging. A noncontacting electrostatic probe head was swept across the face of the sample in ~30 to 40 s. The probe head (TREK Model 4052E) has a sensing aperture 1.3 mm (0.05 in.) in diameter and is maintained ~6.4 mm

(0.25 in.) from the sample front surface. The track of the probe across the sample is shown in Figure 9 (as seen from the electron gun). When the probe is not sweeping, it rests out of the beam over a grounded metal plate. The probe head is mated to a TREK Model 340 HV electrostatic voltmeter. The output of this voltmeter, together with a probe position indicator, were recorded on an Omnigraphics X-Y plotter.

As a check on whether the concurrent operation of the electron beam affected the accuracy of the surface potential data, TREK-probe measurements were performed with the beam uninterrupted and also with the beam temporarily shut off (during the time required to perform a sweep). No difference was observed in the recorded measurements except for the slight integrated loss in charging while the beam was off.

2.1.4.2 Current Measurements

Several current measurements were made in these tests:

- Beam current density measurements. This measurement is made with the Faraday cup described in Section 2.1. It can be moved in front of the sample as it is charged to sample beam uniformity and beam spreading. The track of this probe across the sample face is shown in Figure 9.

- Sample leakage current. This is the primary experimental measurement and is obtained from an electrical connection to the sample mounting plate. The reading is a combination of bulk and surface leakage currents and a displacement current, which exists while the sample is being charged.

- Wall current. An electrically isolated copper baffle in the sample test section is used to obtain this reading, which is used as an indication of beam spreading.

- Witness current. This reading is obtained using a fixed Faraday cup mounted off-axis in the main chamber. The purpose of this reading is to monitor the beam characteristics during the test.

All current readings were taken with digital picoammeters (Keithley Model 480).

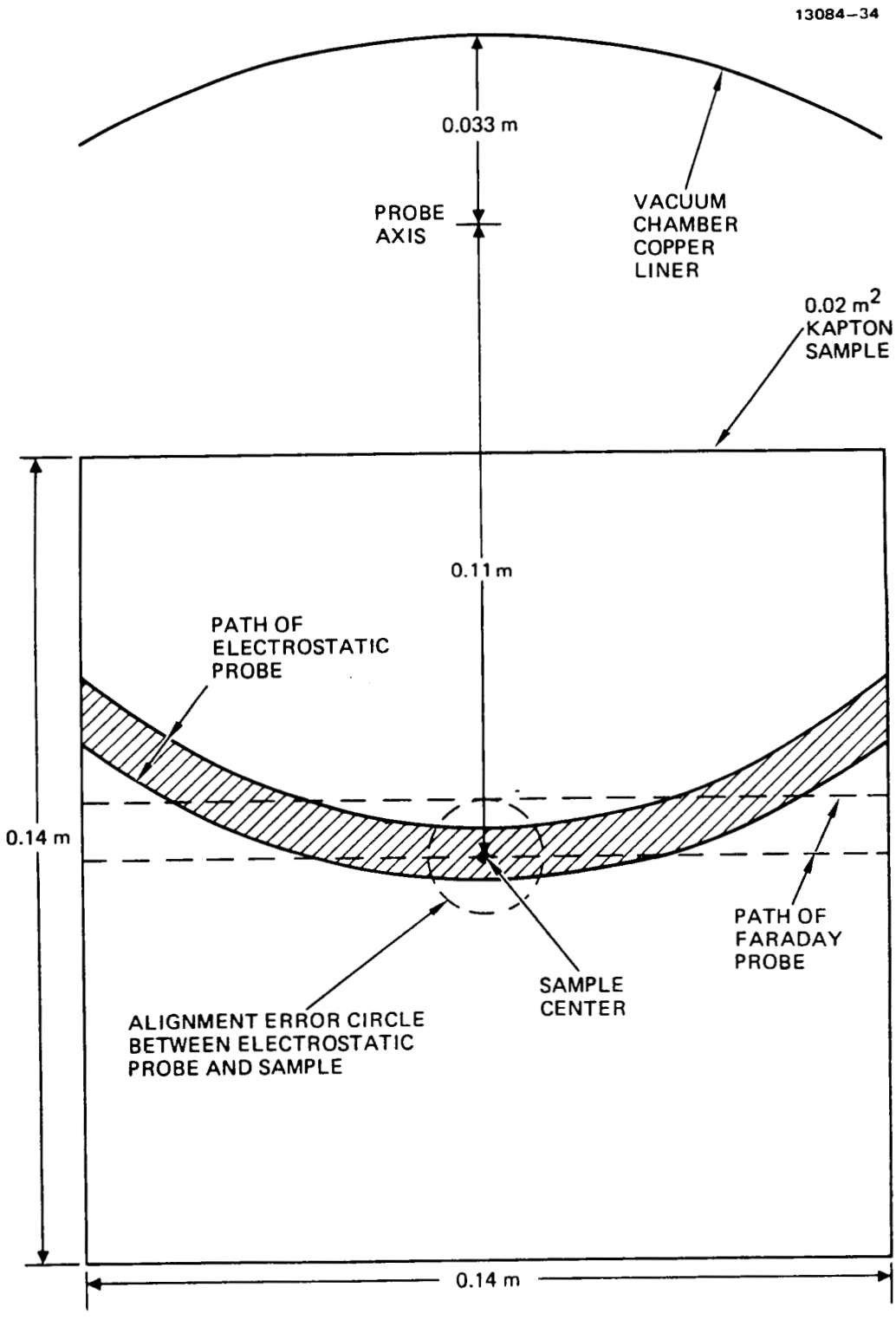

Figure 9. Sample and probe geometry.

2.1.4.3 Data Recording

Data recording was accomplished with the aid of an Apple II microcomputer. A real-time clock installed in the computer was used to provide timing data. At set intervals of time (usually 0.01 h) the computer read and recorded all currents and the time. When the TREK probe sweeps were initiated, the computer noted it on the data printout. Since the computer allowed comments to be inserted on the printout, a comprehensive record of the tests and comments was obtained from the computer output and the X-Y plots of surface voltages.

2.2 EXPERIMENTAL PROGRAM

2.2.1 Test Procedure

The procedure given here is for electron-irradiation tests at normal incidence.

The purpose of the tests was to measure leakage currents and surface potential profiles as a function of time at a given set of beam voltages and currents. All measurements were made in the dark and care was taken to prevent light exposure between measurements as well as for a period over 24 h prior to the first measurement to prevent the photoconductivity effect in Kapton from dominating the results.

The following test procedure was used:

- For a test on an uncharged sample, the Faraday cup was positioned at the sample center, the beam energy preset to the desired value, the gun turned on, and the filament current adjusted to obtain the desired current density. After achieving the desired density, the Faraday cup was retracted. The time to set the desired electron gun characteristics was minimized by using calibration settings to avoid nonrepresentative charging effects caused by improper gun settings and the presence of the Faraday cup.

- The sample leakage current, wall current, and witness current were recorded every 0.01 h (36 s) using the real-time clock in the computer data acquisition system.

The surface-voltage probe was swept across the sample periodically (manual commands). The profile was recorded on the X-Y plotter and the time was noted on the trace and the computer record. The voltage measurements were timed to occur between successive current readings.

- Testing was continued at each beam voltage until equilibrium was reached. Equilibrium was defined as that time when minimal changes in surface voltages occurred. At the lower beam energies, reaching equilibrium required one to two hours. At the highest beam energies, up to five hours were required to stabilize the readings.

- Following each experimental run, the sample was "decharged" by gradually reducing the electron-beam energy while maintaining the leakage current slightly positive. This procedure resulted in a decharging rate of approximately 5 to 10 V/s until the surface voltage reached ~4.5. At this point the rate dropped to 1 V/s. This process generally reduced the surface voltage to zero in one to three hours for tests in which the beam energy was <8 kV. For tests >8 kV, a residual surface voltage of -100 to -200 V remained that could only be removed by exposing the sample briefly to air.

- Tests were always run with beam energies in ascending order (i.e., 2, 4, 6, 8, 10, 12, and 14 kV).

The desired current density for conducting these tests was 3 $\mu A/m^2$. This value was set prior to the start of each test. However, the extremely long times to reach equilibrium (see Section 2) led us to question the Faraday cup measurement system. Subsequent recalibration of this system resulted in the determination that an error did exist in the reading and that this error varied with beam energies. Hence, the tests were not run at the same initial current density, but at values listed with the data.

2.2.2 Experimental Results

2.2.2.1 Data

The data reported in this section was obtained from a continuous series of runs lasting over a period of 33.5 h. The test procedures outlined previously were followed (i.e., tests

were run with increasing beam energies and the sample was decharged between runs).

The maximum surface voltage reading and leakage current as a function of test time, along with the transient surface voltage profiles, are shown in Figures 10 through 23 and are summarized in Table 1 for the various beam energies. While the data for the leakage currents were obtained every 36 s, only data points three minutes apart were used for the figures. This was an arbitrary choice to keep the plots readable. The maximum surface voltage plots represent all of the TREK probe sweeps. The surface voltage profiles given are a representative grouping to illustrate the general behavior.

The 14 keV beam energy test produced what appears to be reasonable surface voltage data, but the leakage currents recorded by the computer were random signals over much of the test period (see Figure 22). Since all other currents recorded were intelligible, it is assumed that the Kapton surface experienced an almost continuous series of microdischarges which generated sufficient noise to cause the computer to record the random signals. In other words, the computer experienced a spacecraft charging anomaly.

Another test was run with the beam energy at 1 keV, but the gun parameters drifted too much to give reasonable transient data. The only reliable result from this test is that the peak surface voltage, at equilibrium, remained negative at a value of about -20 V.

The other currents obtained in this test were recorded and screened as part of the data review. Since these currents do not influence the conclusions drawn from the tests, they have not been plotted.

2.2.2.2 Discussion

From the data that were obtained in these tests there are several areas that warrant further discussion.

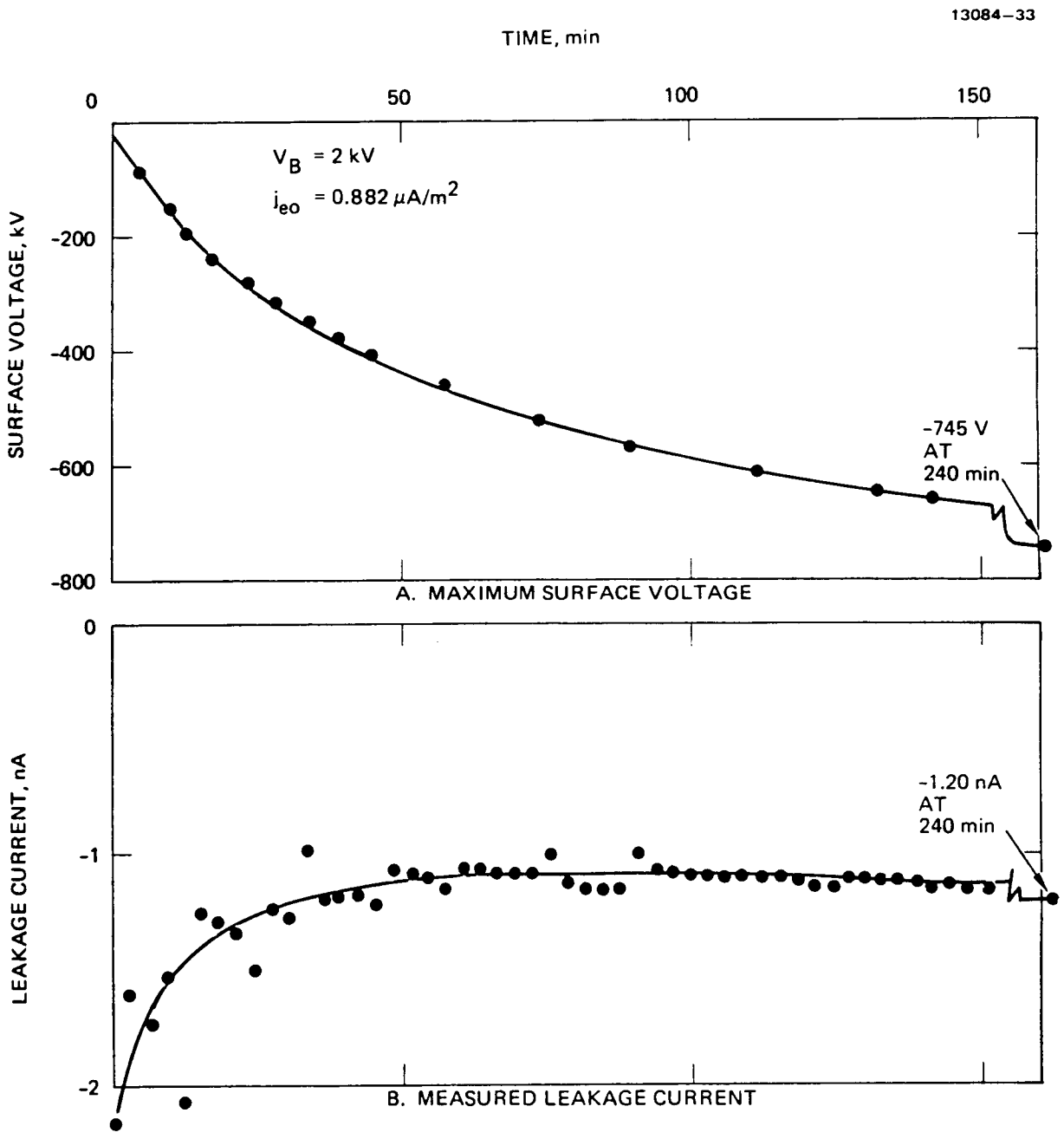

Figure 10. Experimental results.

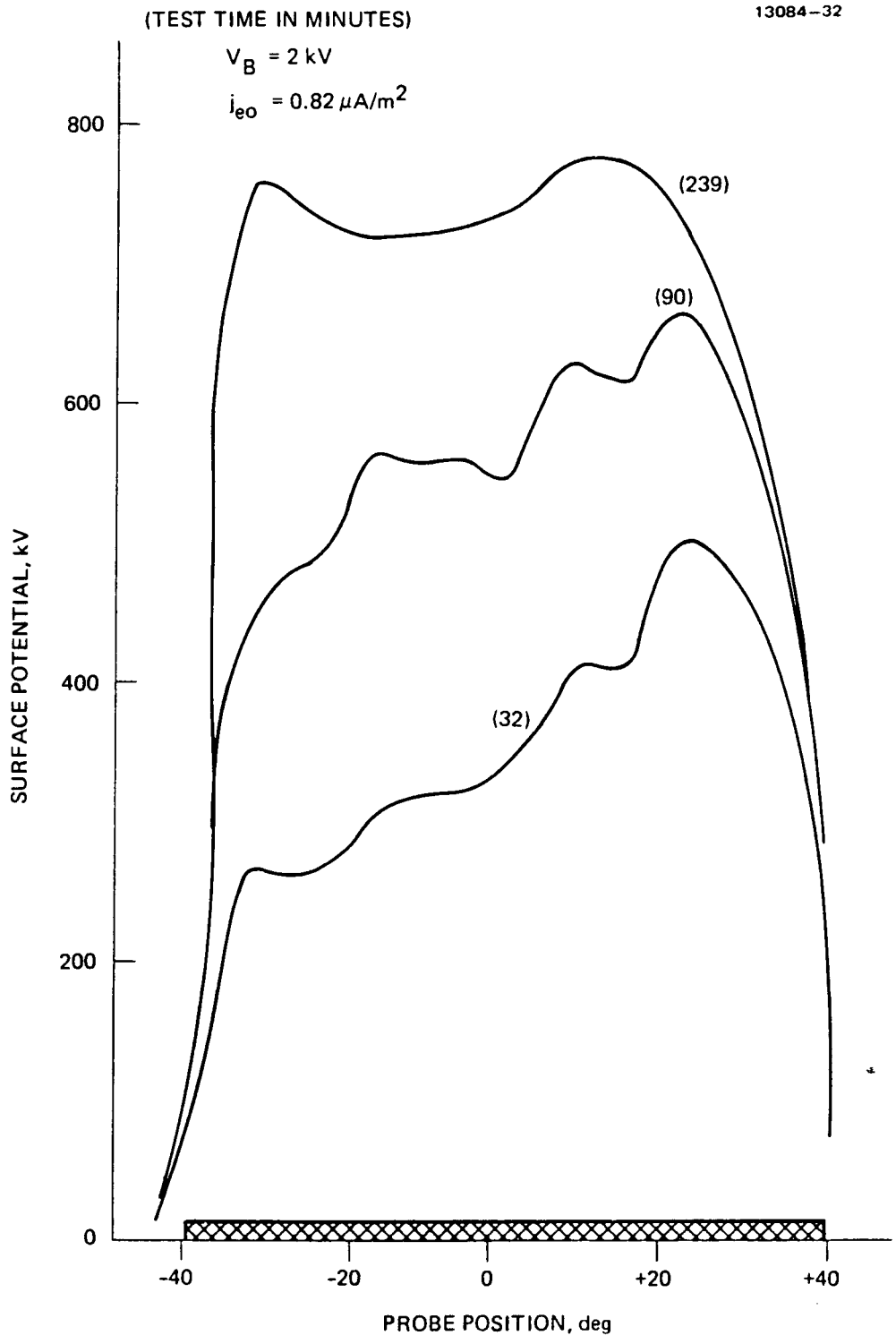

Figure 11. Surface charging profiles.

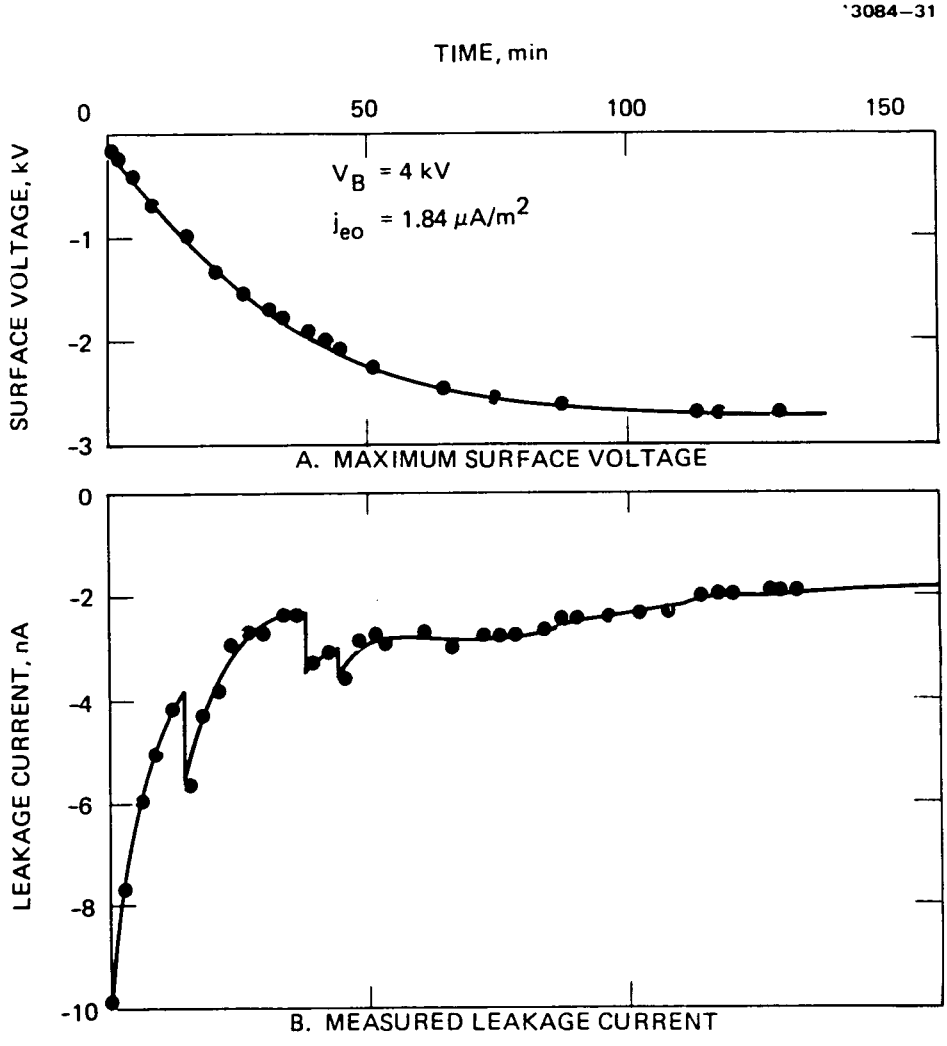

Figure 12. Experimental results.

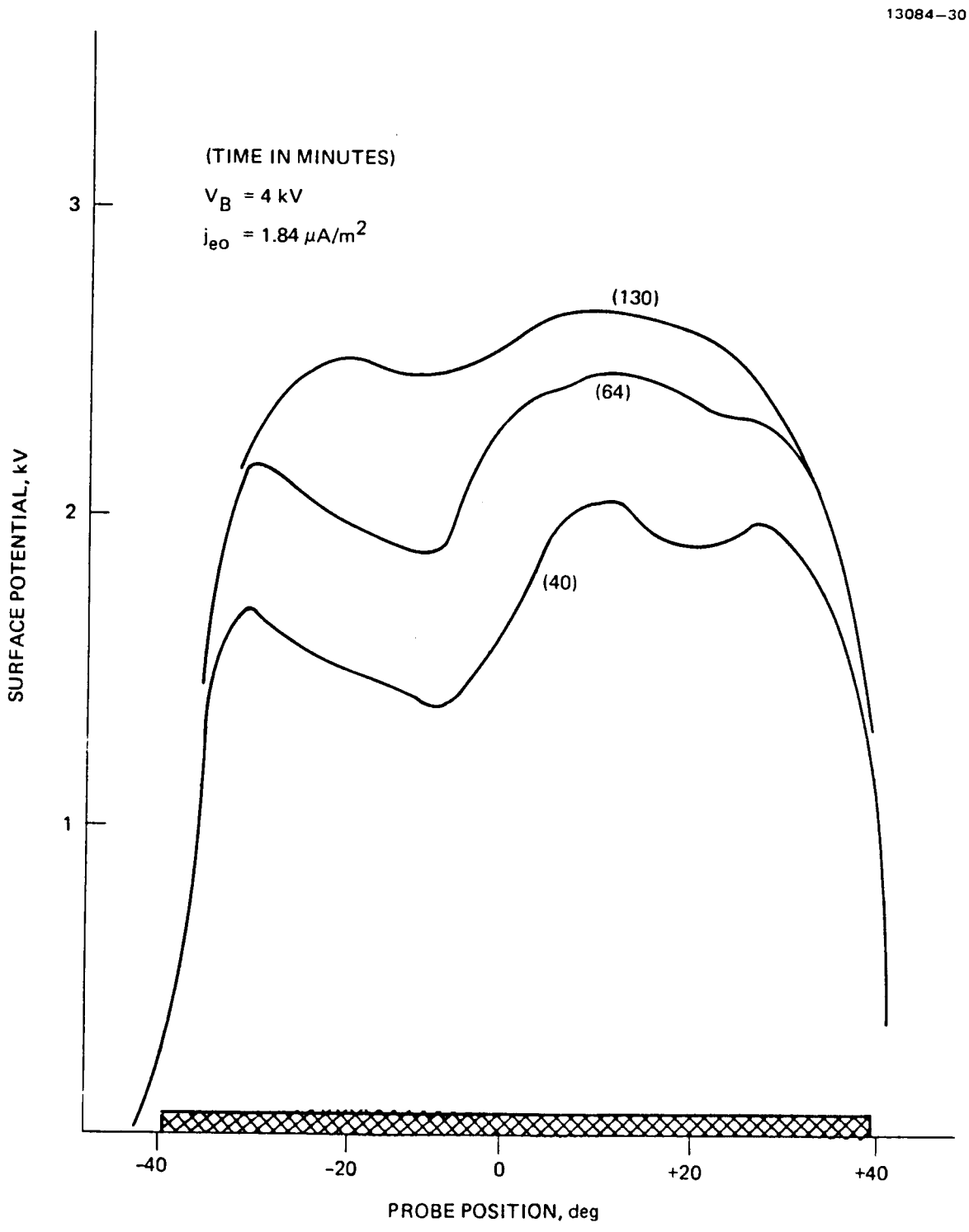

Figure 13. Surface charging profiles.

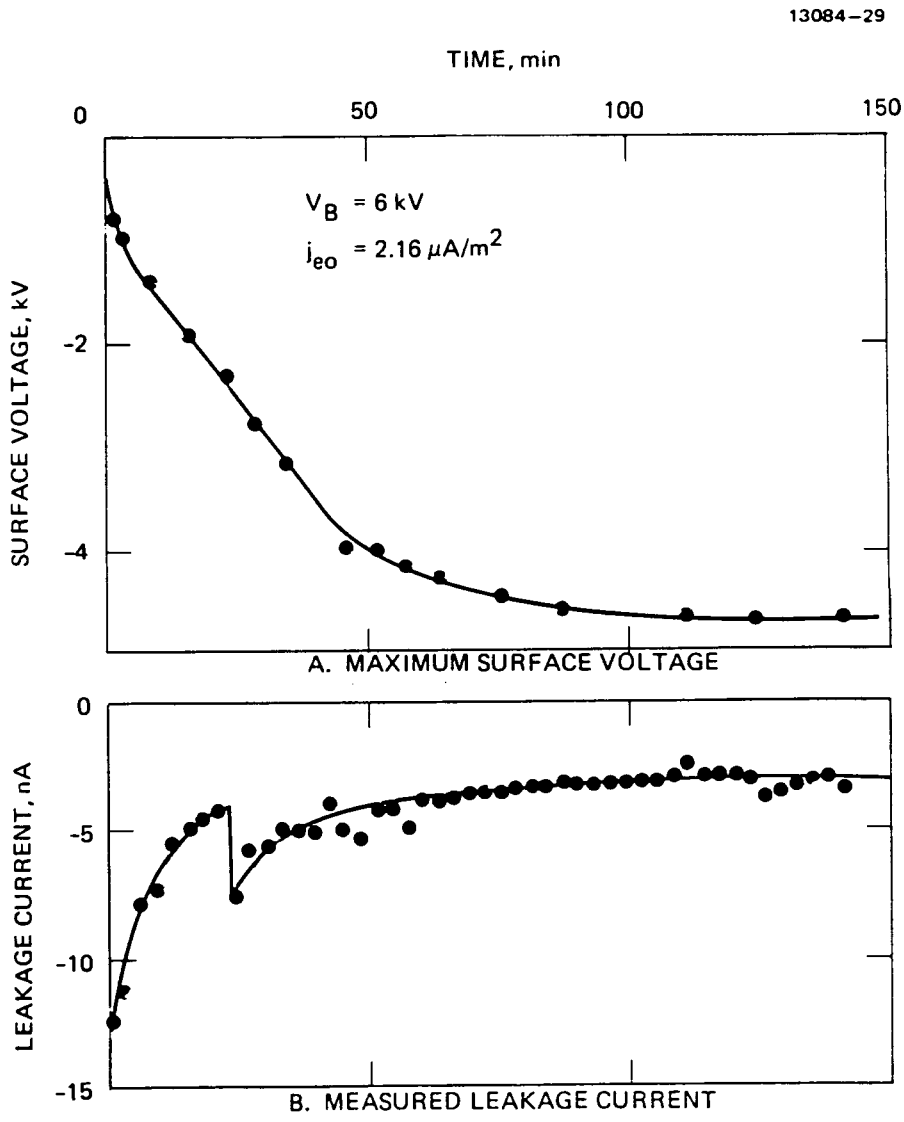

Figure 14. Experimental results.

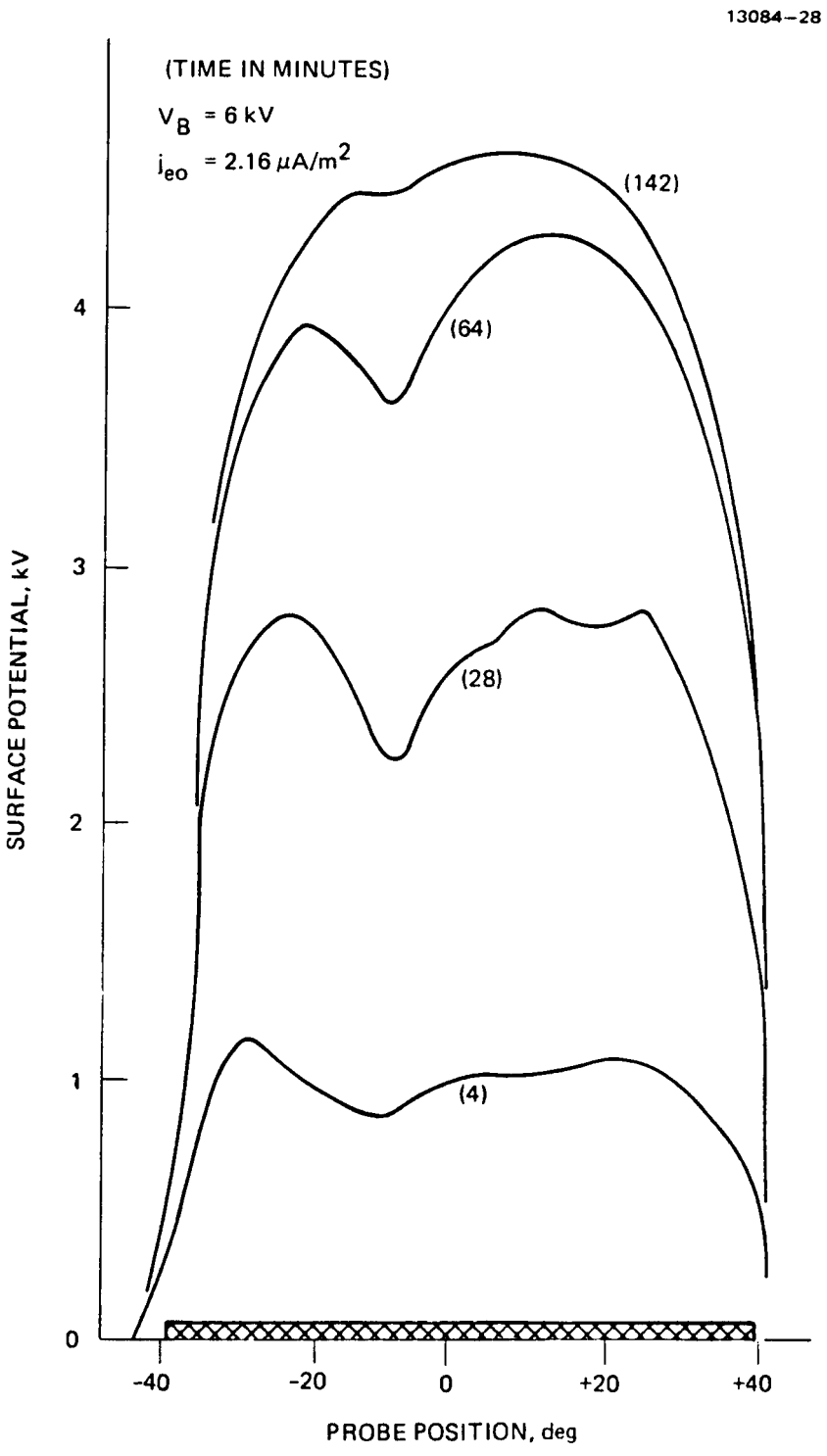

Figure 15. Surface charging profiles.

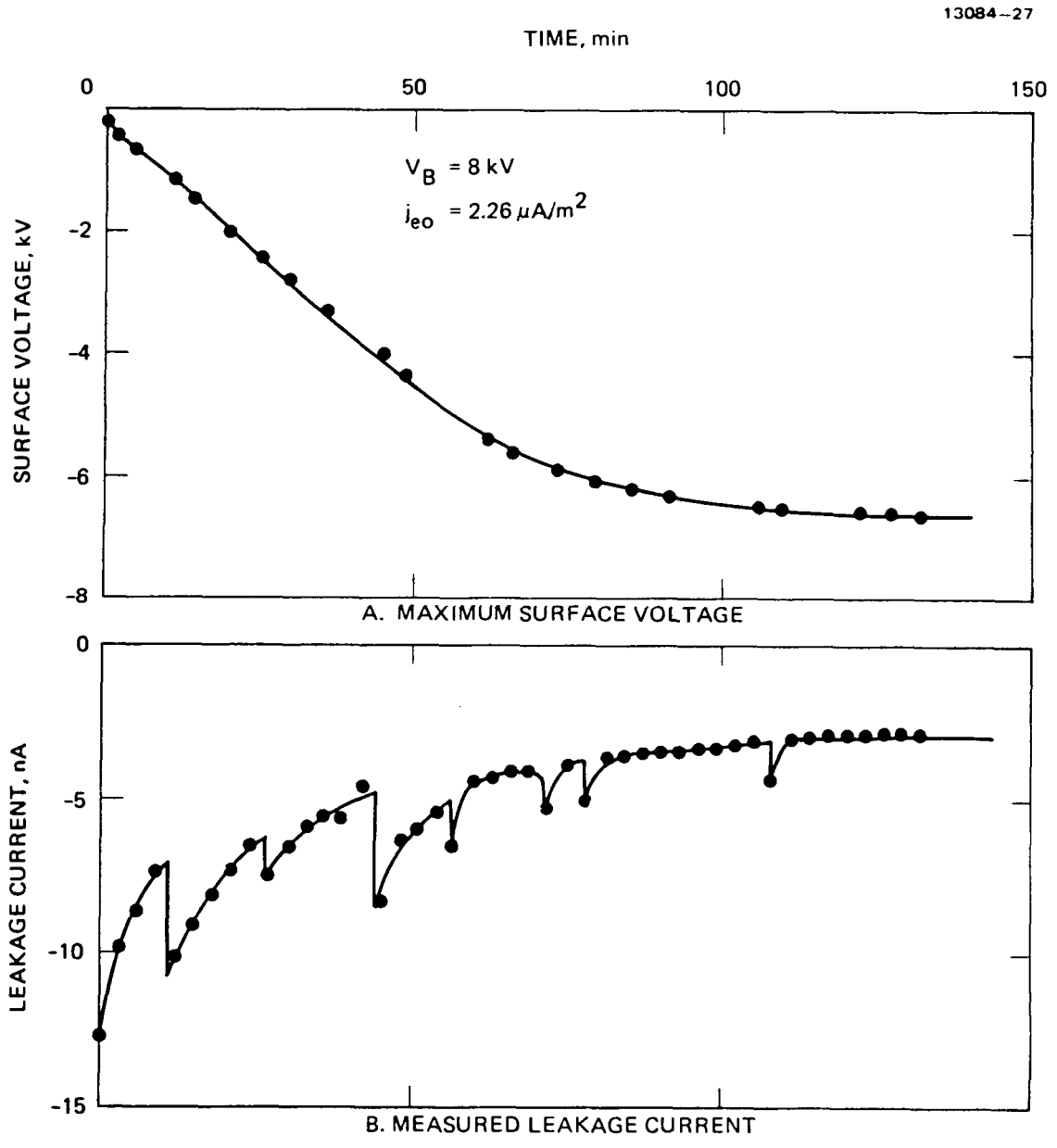

Figure 16. Experimental results.

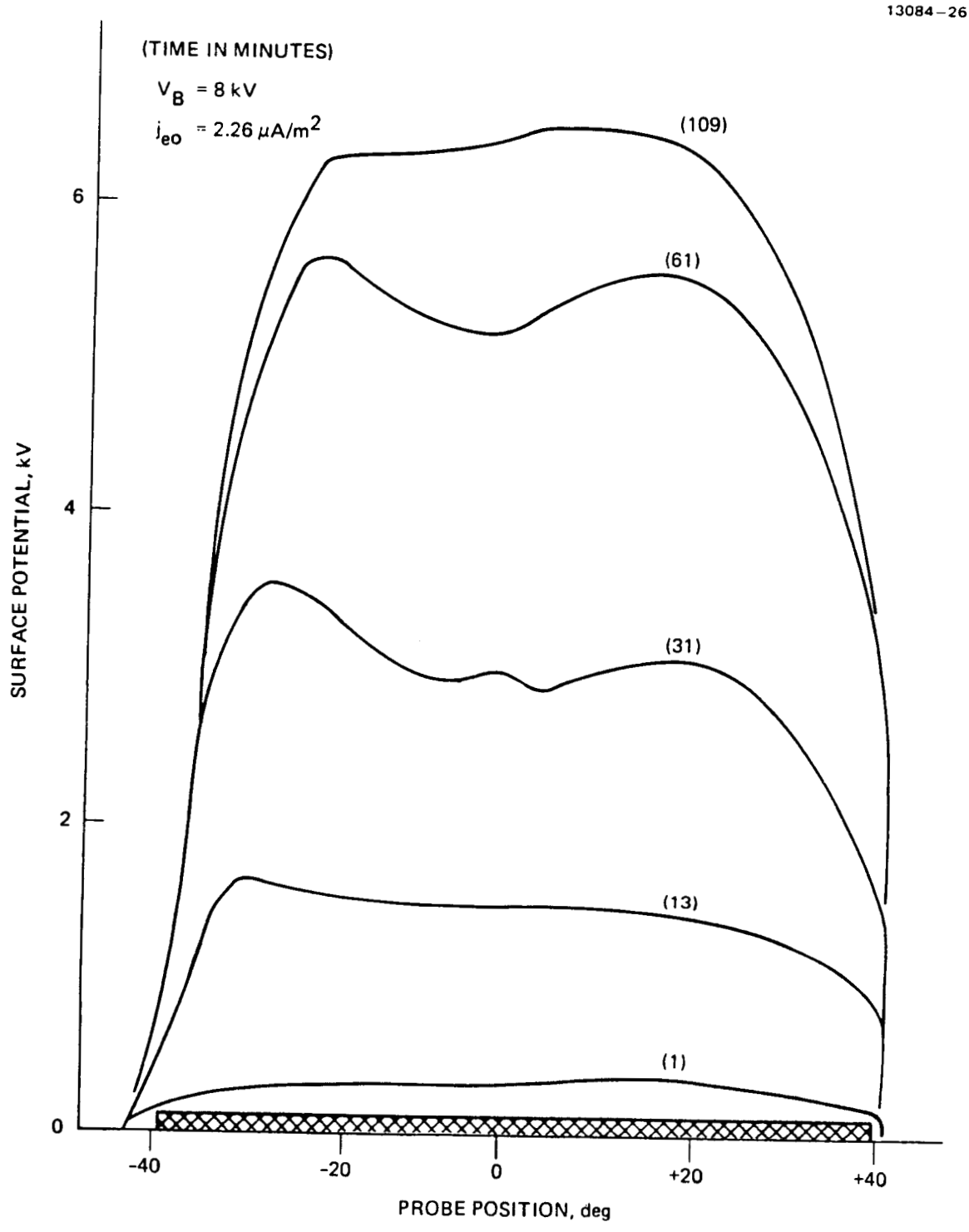

Figure 17. Surface charging profiles.

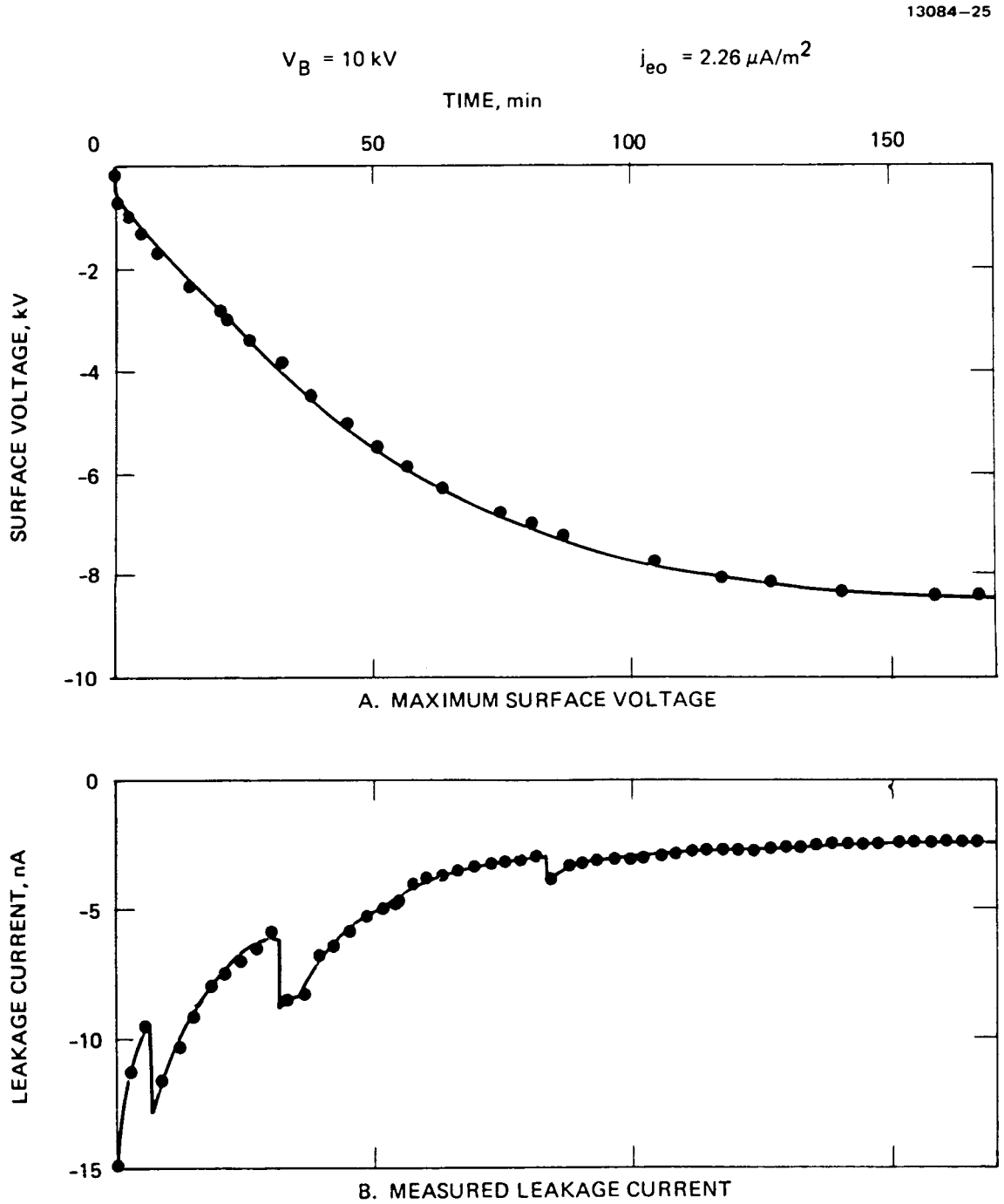

Figure 18. Experimental results.

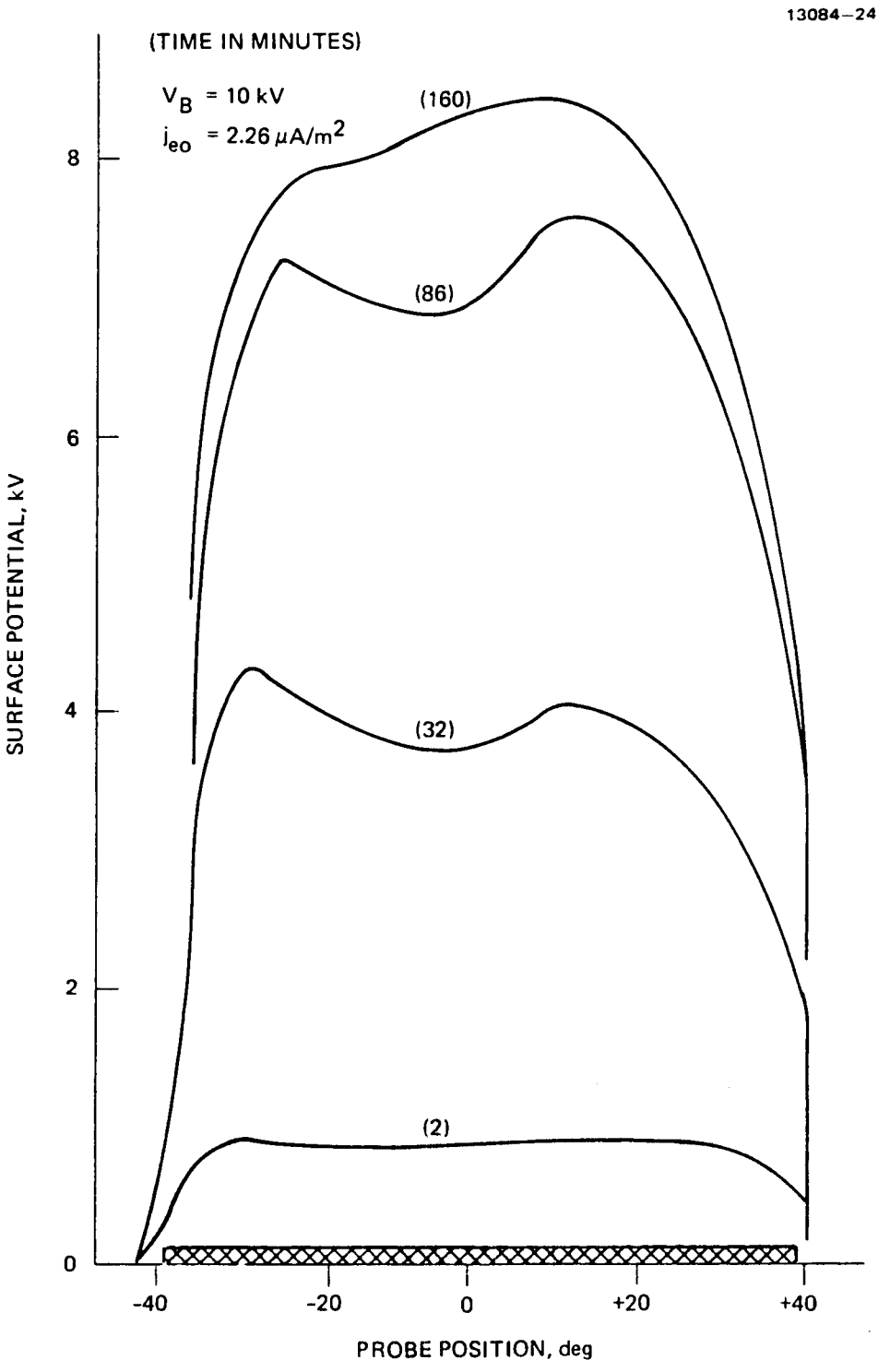

Figure 19. Surface charging profiles.

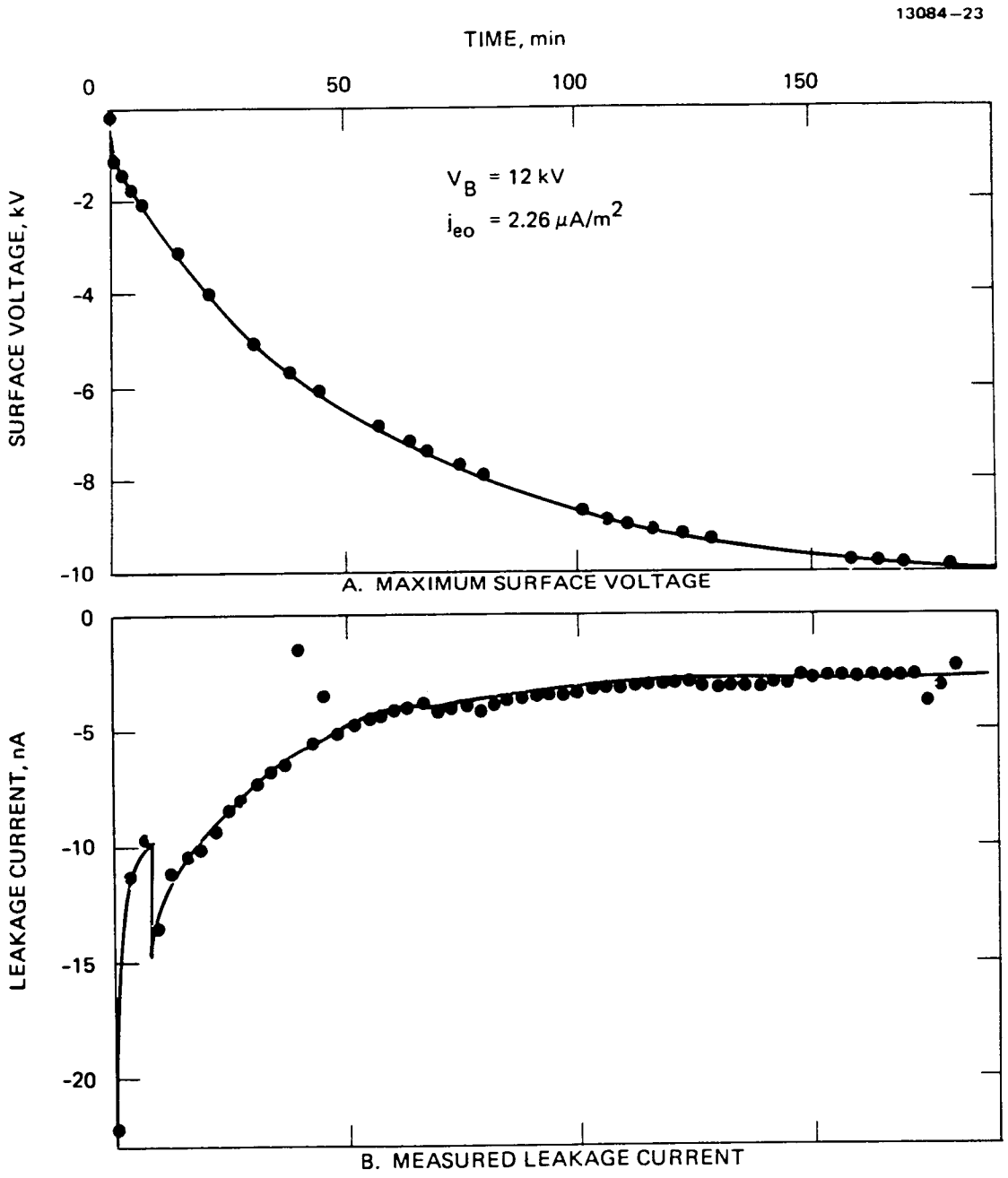

Figure 20. Experimental results.

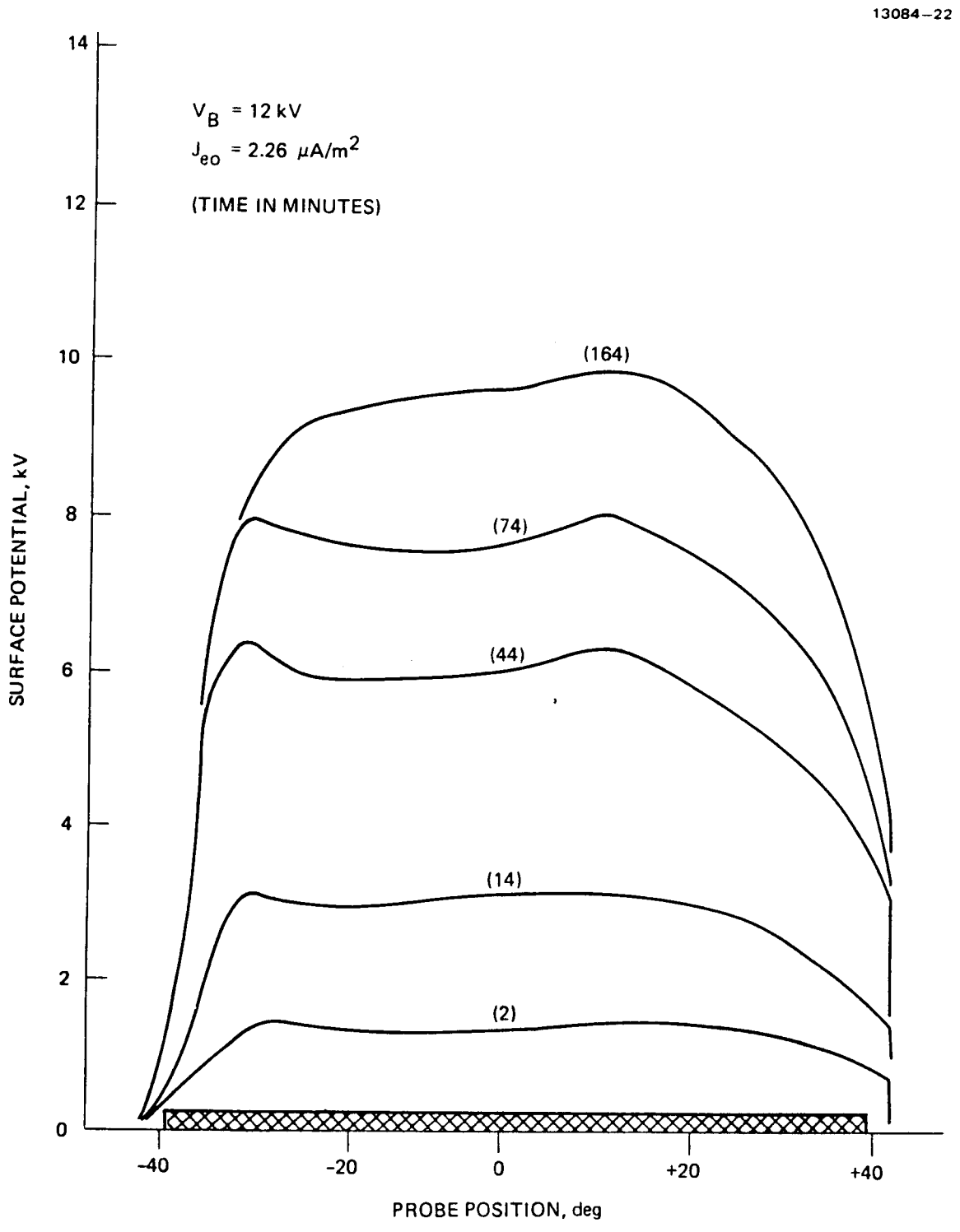

Figure 21. Surface charging profiles.

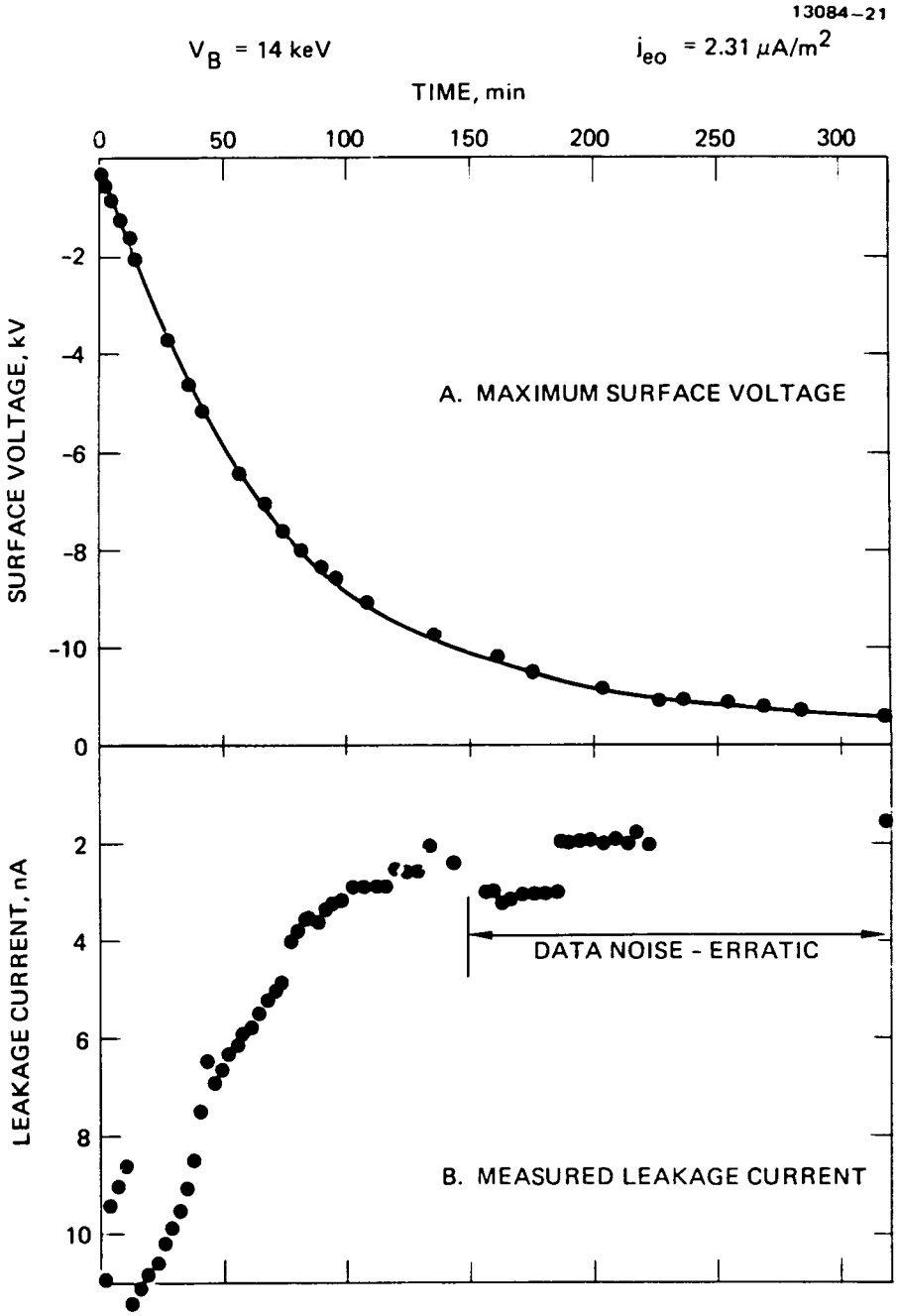

Figure 22. Experimental results.

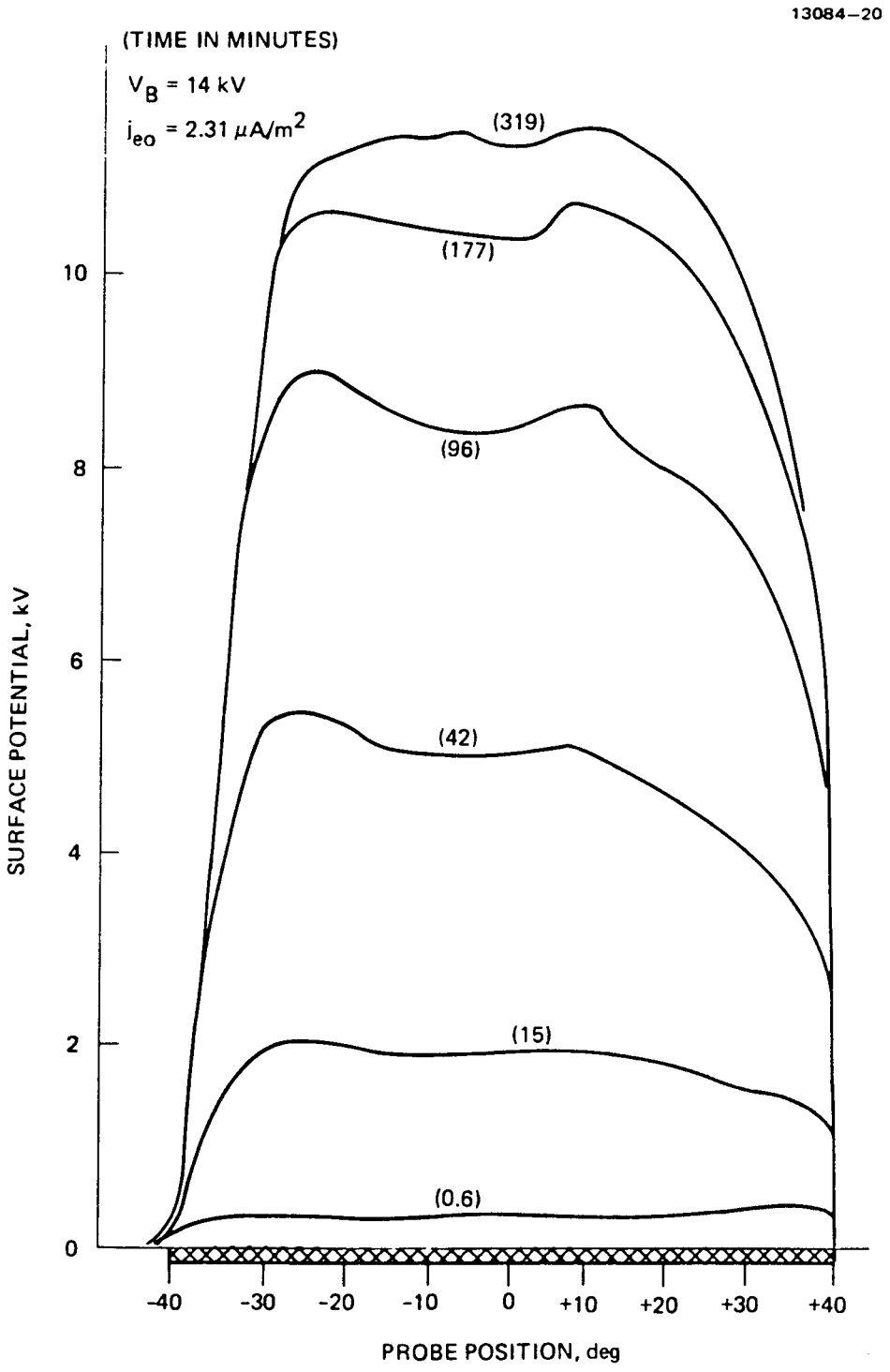

Figure 23. Surface charging profiles.

TABLE 1. Summary of Experimental Results and Derived Properties.

DATA					DERIVED PROPERTIES						
BEAM		SURFACE VOLTAGE			CONDUCTIVITY		DIELECT. CONSTANT		TOTAL YIELD		
ENERGY keV	INITIAL CURRENT DENSITY $\mu A/m^2$	MAXIMUM VALUE kV	AVERAGE VALUE kV	LEAKAGE CURRENT I_L, nA	EFFECTIVE RESISTANCE Ω	EFFECTIVE CONDUCTIVITY S/m	CHARGE μC	κ	V_B-V_S kV	INCIDENT CURRENT DENSITY $\mu A/m^2$	TOTAL YIELD ϵ_R
-1.0	--	-0.018*	--	1.2	(1.5×10^{10})	(423×10^{-15})	--	--	0.982	0.7	0.924
-2.0	0.882	-0.750	-0.590	1.2	4.9×10^{11}	13×10^{-15}	3.71	4.51	1.25	0.697	0.890
-4.0	1.84	-2.70	-1.73	1.8	9.6×10^{11}	6.6×10^{-15}	9.94	4.12	1.30	1.05	0.866
-6.0	2.16	-4.65	-3.16	3.0	1.1×10^{12}	5.8×10^{-15}	14.8	3.36	1.35	1.02	0.792
-8.0	2.26	-6.64	-4.91	3.0	1.6×10^{12}	4.0×10^{-15}	21.8	3.19	1.36	0.93	0.775
-10.0	2.26	-8.50	-6.29	2.4	2.6×10^{12}	2.4×10^{-15}	29.4	3.35	1.50	0.88	0.815
-12.0	2.26	-10.3	-8.65	2.8	3.1×10^{12}	2.1×10^{-15}	31.7	2.63	1.70	0.85	0.804
-14.0	2.31	-11.4	-- +	-- +	--	--	--	--	--	--	--
					AVERAGE	5.7×10^{-15}		3.53			

* 1-keV Beam Data Did Not Exhibit Nominal Charging Characteristics

\+ 14-keV Beam Data Not Reduced Due to Noise on Leakage Current Record

- Equilibration Time. At the current densities used in these tests, it required 2 to 5 h to reach equilibrium surface potentials. When the current density for a 2-keV beam energy test was inadvertently increased by a factor of five, the charging rate also increased by about the same amount (see Figure 24 for the comparison of these two surface voltage transients). Yet, when this data is compared to data taken at the NASA Lewis facility on Kapton under 10 $\mu A/m^2$ current densities, there is a discrepancy: the Lewis sample charges to equilibrium in under 10 min. This implies that the sample tested here under low beam current densities should have reached equilibrium in 1 to 2 h. This question of different charging rates is discussed further in Section 3.

- Leakage Currents. The leakage current data exhibits the characteristics of a capacitor being charged, as expected. In the 2-kV beam tests (Figure 10), there is considerable oscillation in the data as the test is initiated. The data shown in Figure 10 (in which the points correspond to 3-min. intervals) show this oscillation clearly. We believe this is due to difficulty with gun operations at low beam voltages.

For all tests above the 2-kV level, the leakage current data show evidence that arcing occurred. The characteristics observed show an abrupt change in the current curve followed by a resumption of the charging curve. There does not seem to be a consistent pattern for the discharges – except that by the time that the 14-keV beam energy test was conducted, the intensity of the noise disrupted the operation of the digital data acquisition system.

Some of the discharge pulses indicated in the leakage current occur at the same time as the TREK probe sweep. This could indicate that the probe is initiating the discharge. However, the probe head is biased to the surface potential that it is reading so that no electric field will exist between them (the probe electronics responds faster than the probe sweep rate).

- Surface voltages. When the maximum surface voltage readings are plotted as a function of test times, they form a fairly uniform family of curves (see Figure 25). The exception to this was the 6-keV beam energy test in

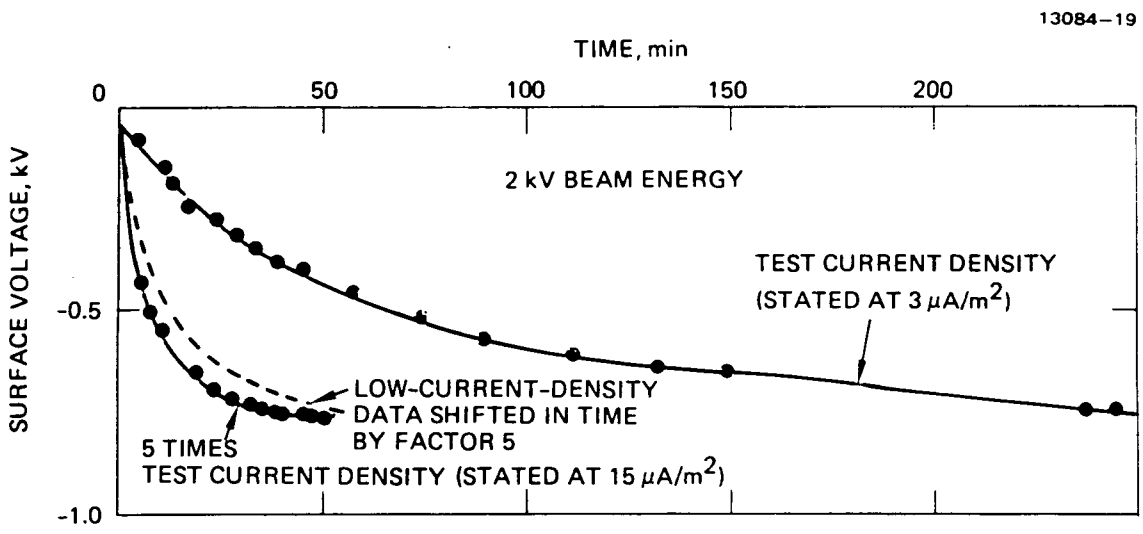

Figure 24. Effect of incident electron current density on charging rate.

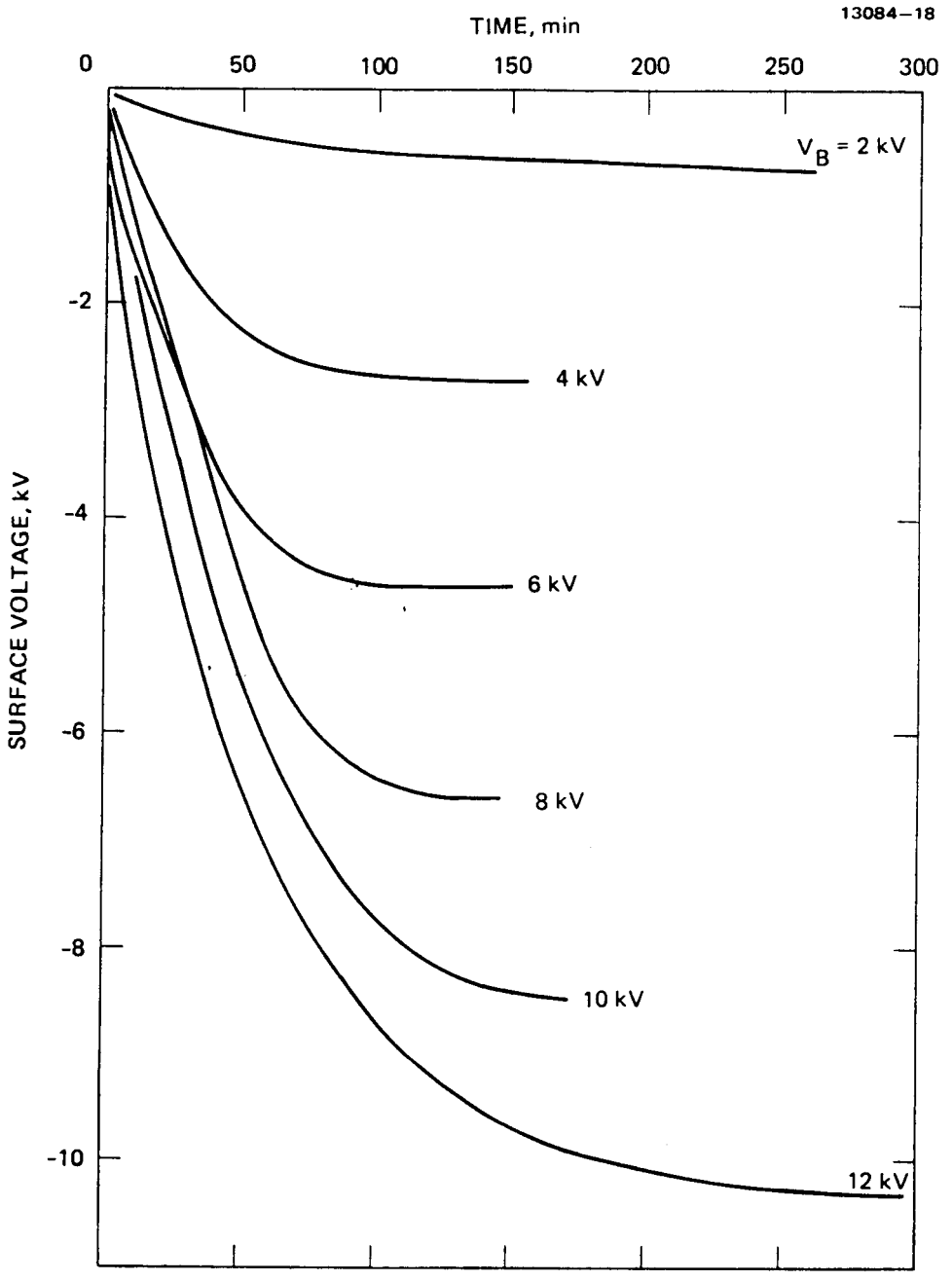

Figure 25. Summary of surface voltage transients.

which the initial electron current density was set too high (by a factor of 100) for the first several seconds. This figure also shows that for beam energies >8 keV, when the sample could not be completely decharged, there is a different initial charging rate. This effect seems to disappear after the first minute of testing.

The surface voltage profiles that were taken (Figures 11, 13, 15, 17, 19, 21, and 23) in the first few minutes of testing (8-keV beam energy tests and above) show an initial uniform charging of the Kapton surface in agreement with the beam uniformity found in the calibration runs. As the surface charging continues, a pattern of peaks and valleys arises. This could be because of nonuniformities in the surface or partial discharges. In equilibrium, the voltage profiles are more uniform, with a characteristic voltage fall-off at the edges. This fall-off is due primarily to beam spreading, resulting in electrons striking the surface at angles, increasing the secondary yields and lowering the surface voltage at the edges.

When plotting equilibrium maximum surface voltage against beam energy, we normally expect a linear relationship, indicating a zero surface voltage at a beam voltage corresponding to the energy required for an incident electron to produce a unity yield.[11] As shown in Figure 26, there is a linear relationship between the beam voltages and the equilibrium surface potentials.

Extrapolating the curve to zero surface voltage indicates that unity total yield for Kapton occurs at a beam energy of ~1300 eV. However, data from experiments for 1-keV beam energy show the surface still negative at about -18 V. Furthermore, the data from other experiments[13,17] on the total yield from Kapton indicates that beam voltages of 750 to 950 V produce unity yields. Therefore, it is evident that something is happening with Kapton samples under low beam energy irradiation that is not completely understood. This should be studied further.

At beam energies >15 keV, the equilibrium surface voltage as a function of beam energy again deviates from linearity. We interpret this as resulting from the surface voltage increasing

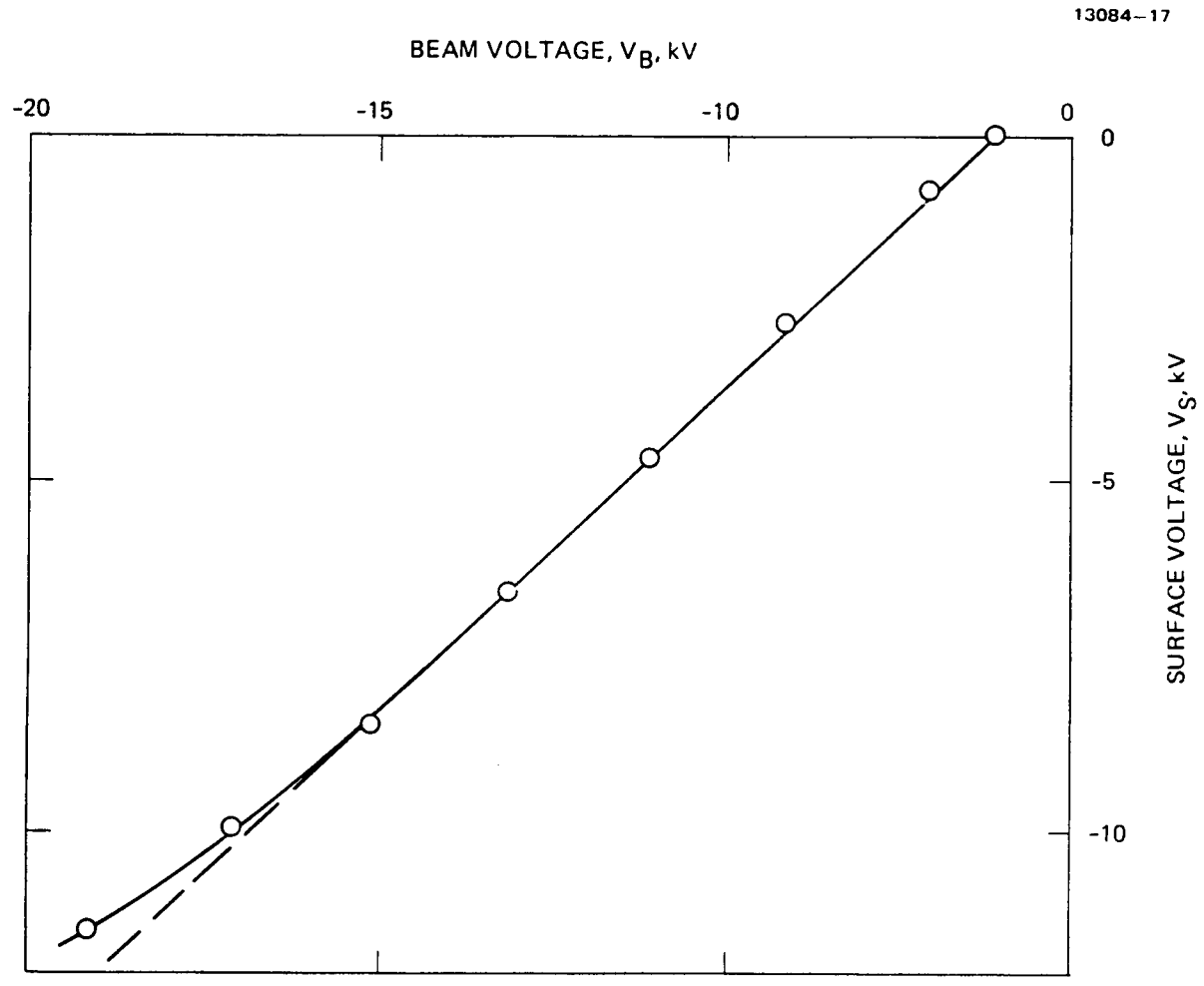

Figure 26. Maximum surface voltage as a function of beam voltage at equilibrium.

to a point where leakage currents start to become a dominant factor in the charging of Kapton (i.e., charging has changed from an emission-limited to a leakage-current-limited process).[18] Comparing the data to other tests conducted at HRL under Internal Research and Development tasks shows that this deviation could be due to leakage currents.

In Figure 27, the effect of electrically floating the substrate is shown. There is a linear relationship throughout the 2- to 14-keV beam energy test conditions. The only difference is that there are no leakage currents. Furthermore, when the leakage currents are increased by decreasing the sample thickness, the linear region can be eliminated, as shown in Figure 28, which compares the 5 mil Kapton behavior to that of 0.25-mil Kapton. Hence, it is conceivable that leakage currents through the Kapton could produce the observed deviation from linearity. Unfortunately, experimental data obtained do not substantiate this. The data show that the leakage currents decrease, and the resulting conductivity computed for high beam energies decreases as well (see subsection 3.1). There is no reasonable explanation for this behavior at this time.

2.2.3 Properties Derived from the Data

The experimental data can be used to derive certain material properties which can be compared to those used by NASCAP. The properties considered here are conductivity, dielectric constant, and total electron yield (i.e., backscattered electrons plus secondary electrons).

2.2.3.1 Conductivity

From the equilibrium-surface-voltage data and leakage-current data an effective resistance can be computed. This value includes both bulk and surface resistance values, which are difficult to separate. Given the sample geometry, it is possible to convert this resistance into an effective value of conductivity by use of:

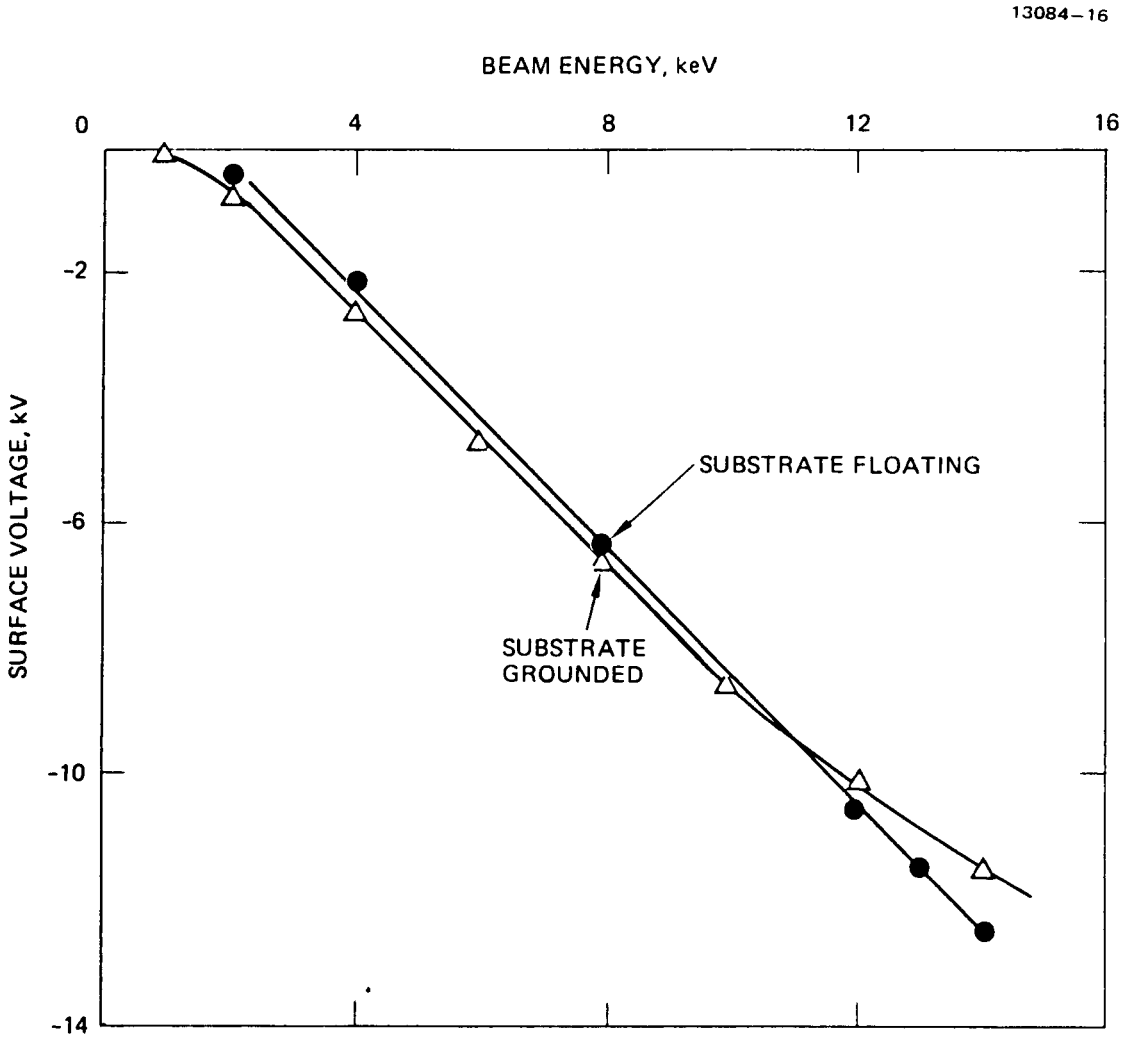

Figure 27. Effect of leakage currents on surface voltage.

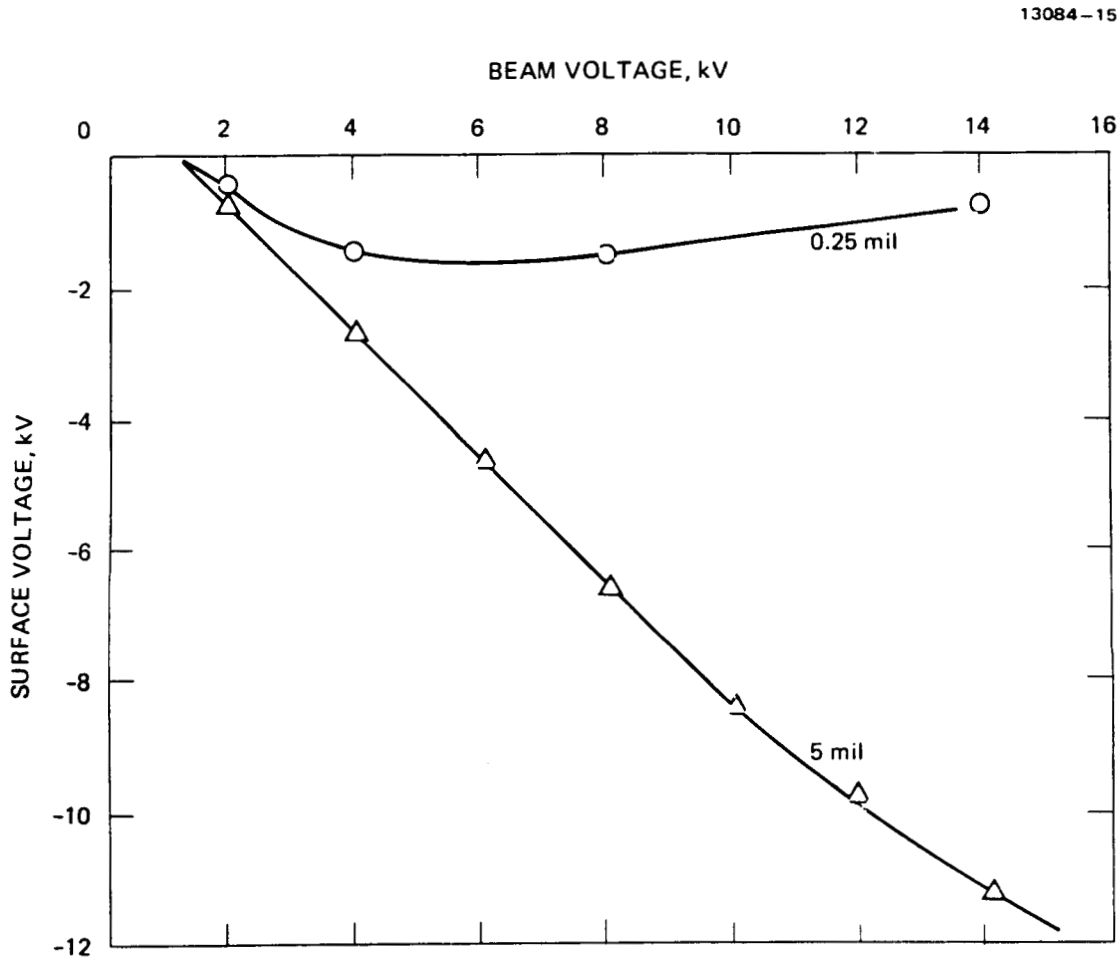

Figure 28. Equilibrium surface voltage values with different Kapton thickness.

$$\sigma_{eff} = \frac{d}{A_s}\frac{1}{R_{eff}} = \frac{d}{A_s}\frac{I_L}{V_s}$$

where d is the Kapton thickness (1.27×10^{-4} m), A_s is the Kapton area (0.02 m^2), I_L is the measured leakage current, and V_s is the average surface voltage.

The problem with this computation is determining the average equilibrium surface potential for the Kapton. As shown on the TREK probe profiles, the surface is not at a uniform potential in the direction of the probe sweep, nor is it expected to be uniform in the direction perpendicular to the sweep. To circumvent this problem, the equilibrium surface voltage trace was integrated to give an average surface potential in the swept direction (see Figure 29). The percentage change between this average value and the maximum measured surface voltage was doubled and subtracted from the maximum value to compensate for the nonuniform surface voltage in the direction perpendicular to the probe sweep. This assumption of the same voltage fall-off at all edges is, at best, a rough approximation, but it is better than ignoring the edge voltages.

The resulting values of the Kapton conductivity are shown in Table 1. As stated previously, the 14-keV beam energy test resulted in noise in the leakage current data. Therefore, material-property values cannot be derived from this test.

The unexpected result immediately obvious from this computation is that the effective conductivity decreases with increasing surface voltages. We anticipated that conductivity would increase. The variation of effective conductivity with sample average surface voltage is shown in Figure 30. As can be seen, a 2-keV beam energy results in the highest value of conductivity, whereas the other results are grouped within a factor of three.

There are three possible explanations for this trend. First, the effect is real and is a result of the exceptionally long period of time that the sample was under vacuum and electrical

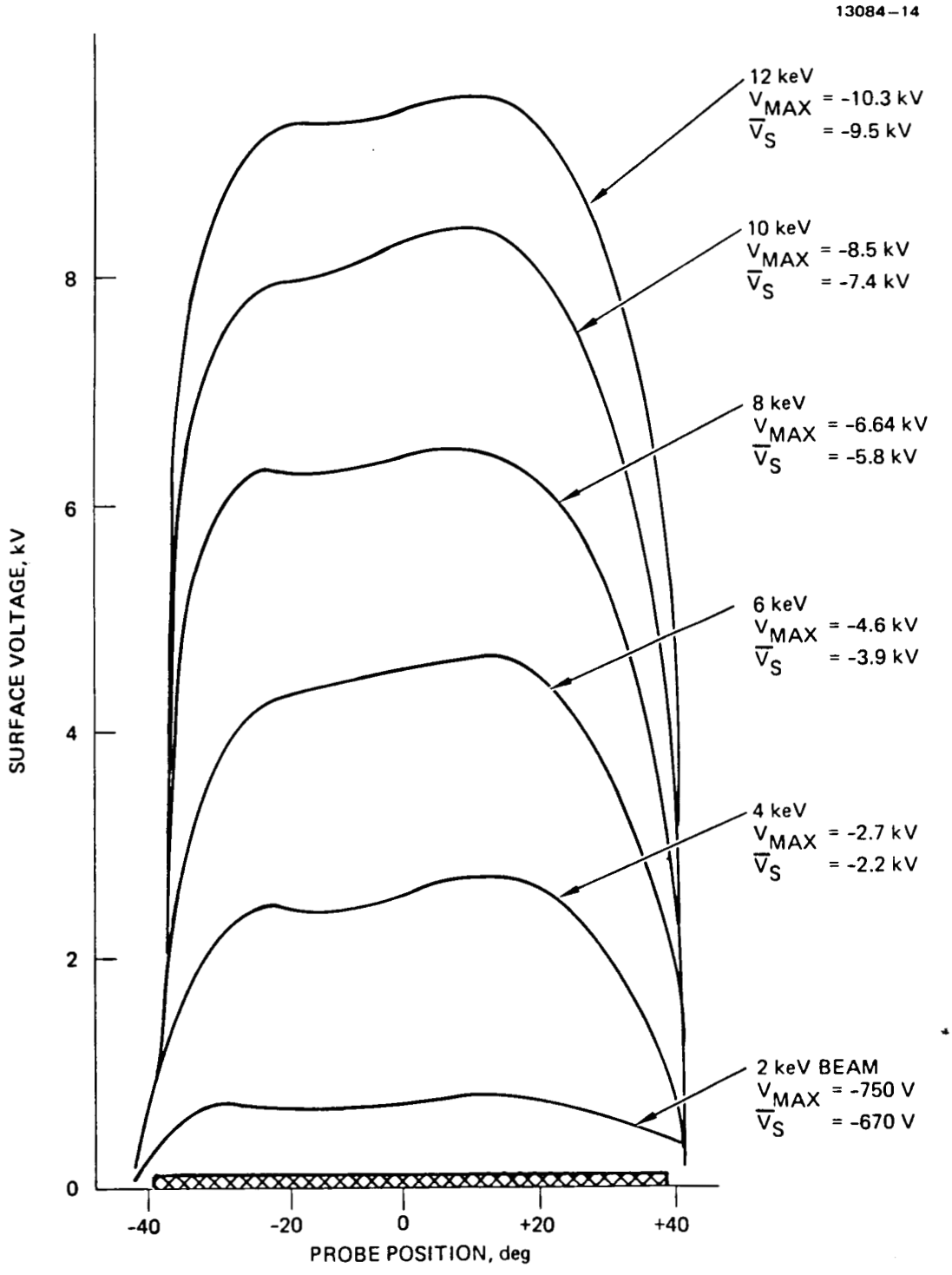

Figure 29. Equilibrium surface voltage profiles.

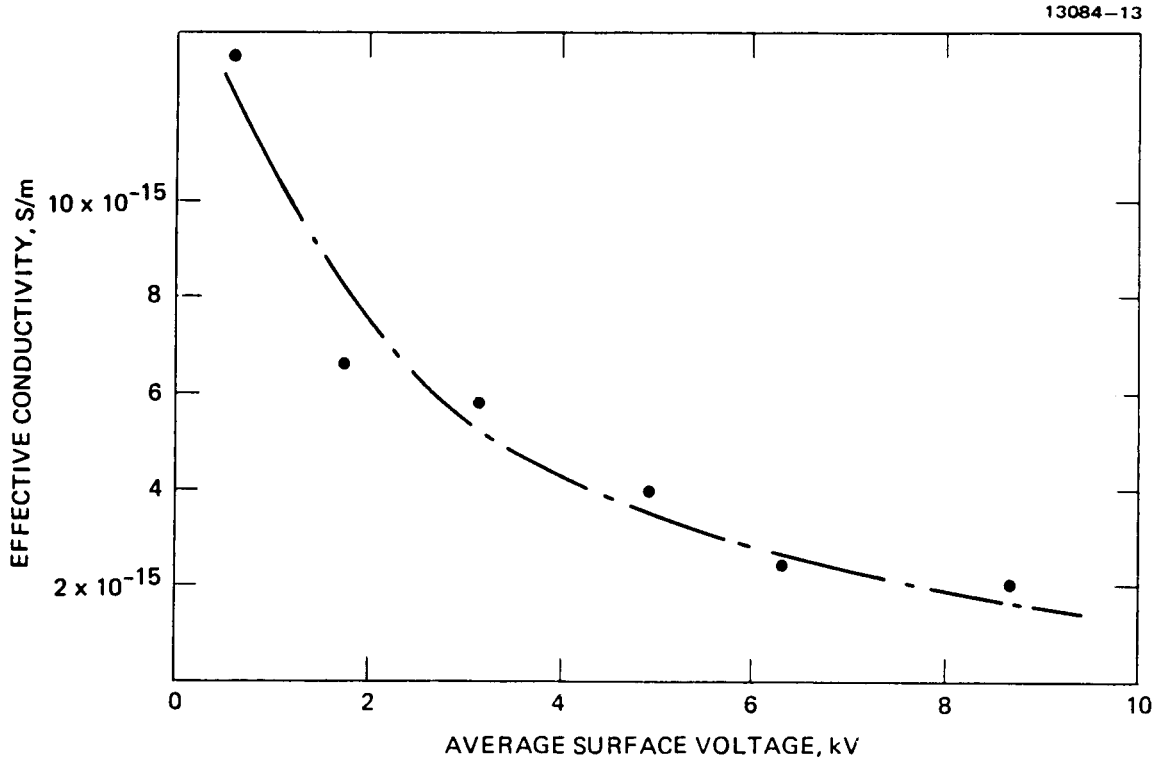

Figure 30. Variation of effective conductivity with average surface voltage.

stress. In a series of tests conducted at Stanford Research Institute, both factors were cited as resulting in decreasing conductivity in Kapton. It was found that conduction in Kapton was primarily an ionic process and was initially due to adsorbed ions which could be depleted, thus changing the material conductivity. Hours under vacuum were required to stabilize the material conductivity at what was believed to be a more characteristic value.

The second possible explanation is that the effective value is really the result of a combined bulk- and surface-conductivity term. With the wrap-around test sample, it is possible to have the surface conductivity change in such a way to cause an overall decreasing conductivity. For example, for this parallel resistance network, if the bulk resistance is constant while the surface resistance increases, then the overall resistance also increases. This produces a decreasing effective conductivity.

The third possibility is that the Kapton sample lifted from the mounting plate. If so, the leakage current would have to flow through a diminished area of contact between the sample and mounting plate which could decrease the current and increase effective resistance. This would result in decreasing conductivity. At this time there is no way to determine what occurred during the test.

The average value of effective total conductivity obtained here is 5.7×10^{-15} S/m. This should be compared to NASCAP values of 3×10^{-15} S/m for bulk conductivity and 2 to 7.5×10^{12} Ω for surface resistivity. Assuming the experiment measured a combined surface and bulk conductivity, and using a bulk resistance value computed from the NASCAP conductivity, the experimental conductivity value could be obtained if the surface parallel resistance was about 2×10^{12} Ω. This agrees with the NASCAP surface resistance value.

2.2.3.2 Dielectric Constant

The dielectric constant for Kapton can be computed from a parallel plate capacitor relationship and the experimental data

$$C = \frac{\epsilon_o \kappa A_s}{d} = \frac{Q}{V}$$

or

$$\kappa = \frac{d}{\epsilon_o A_s} \frac{Q}{V} ,$$

where d is the sample thickness (1.27×10^{-4} m), A_s is the sample area (0.02 m^2), ϵ_o is a constant (8.85×10^{-12} F/m), Q is the charge stored in the dielectric, and V is the voltage across the dielectric.

The voltage across the dielectric is the average equilibrium surface voltage value for each test. For reasons given previously, the 14-keV beam energy data are not considered here.

The charge stored on the dielectric is obtained from the leakage current data. Since this current measurement includes discharge transients and conduction currents through the dielectric and the charge storage, corrections must be made to compensate for these effects. First, the conduction currents are calculated using the equilibrium resistance value and the surface voltage values at specific test times. A curve is then flared through these data points [see Figure 31(a)].

Accounting for the discharge transients is more difficult. This is accomplished by flaring a curve using the initial-slope data points and the final current values. This technique can introduce a considerable tolerance for adjustment in computing the charge stored. The procedure is to draw the curve, after which it would not be changed. We assumed that the average of the six readings would be reasonable. The charge is computed as the area between the two curves.

The computed charge and dielectric constants for each of the six test conditions are given in Table 1. Although the spread is large, the average value is 3.5. This is the value originally

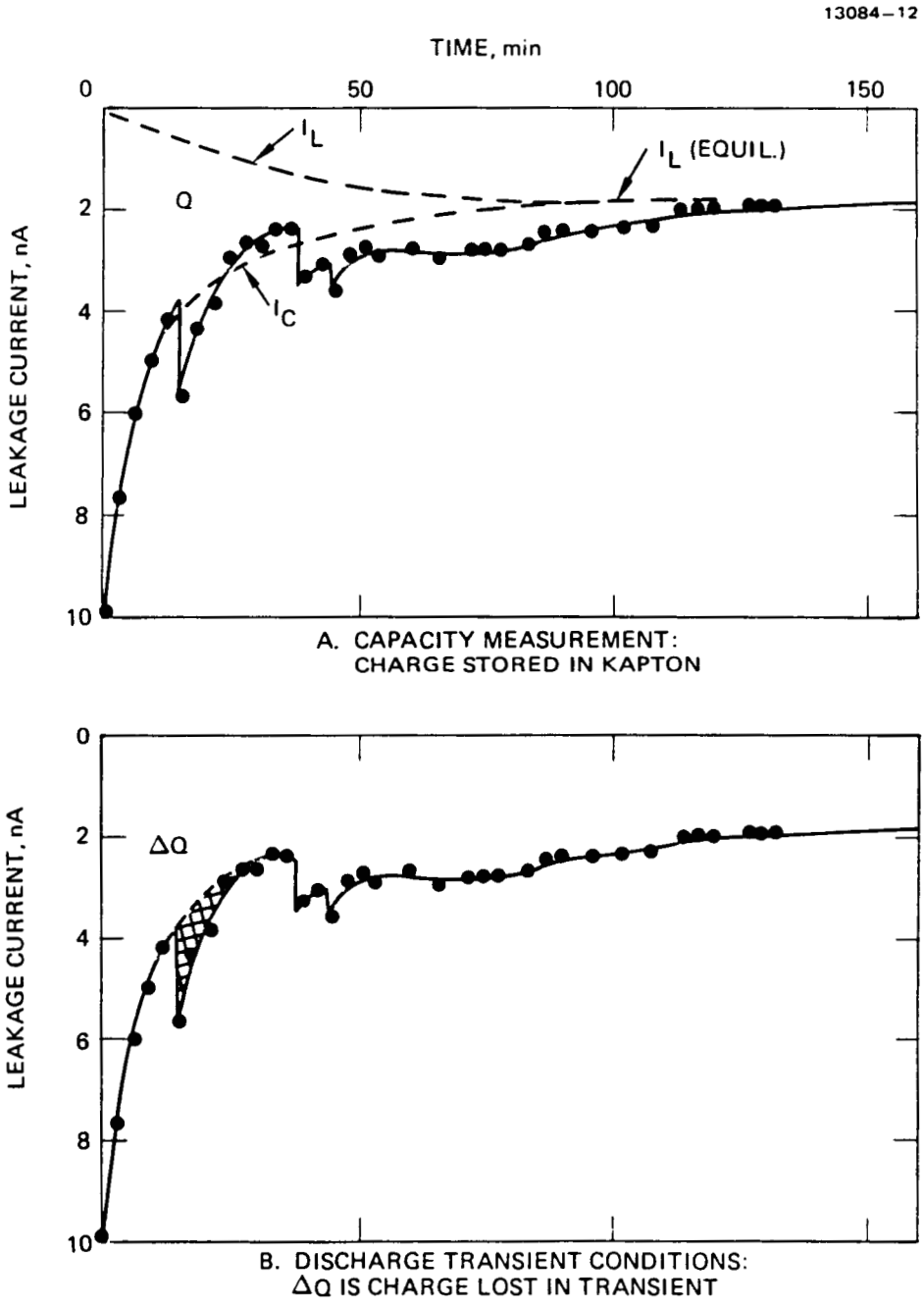

Figure 31. Typical computations from leakage current measurements.

used in NASCAP, but higher than the value of 3.0 quoted for work at the Lewis Research Center.[14]

The technique of integrating the leakage current transients to obtain charge can be used to evaluate the discharge transient conditions [see Figure 31(b)]. The area between the discharge transient and a curve fitted to the expected shape (without a discharge) can be integrated to obtain a measure of the charge lost in the discharge. Using this delta charge (ΔQ) and the parallel-plate-capacitor relationship, the change in surface voltage can be computed. For the example shown in Figure 31(b), we found that

$$\Delta Q = 0.7\ \mu C \text{ and}$$
$$\Delta V_s = 140\ V.$$

The voltage change given here is over the whole surface. If the discharge were localized, then the change in voltage would be considerably larger. If this type of discharge occurred in a nominal discharge transient time of ~200 ns, then the current transient would be ~3.5 A. Hence, it would be a little-bang category of discharge which are now believed to be the principal cause of charging-induced anomalies.[19]

2.2.3.3 Total Yield

The basic relationship that governs the charging of surfaces is a current balance. If charging a sample in the dark using only electrons is considered, then the relationship is

$$(I_e)_{in} = (I_e)_{sec} + (I_e)_{BS} + (I_e)_{cond} + (I_e)_{stored}$$
$$= (I_e)_{ty} + (I_e)_{cond} + (I_e)_{stored}$$
$$= \epsilon_R (I_e)_{in} + \frac{\Delta V}{R} + C\frac{dV}{dt},$$

where

$(I_e)_{in}$ is the incident electron current to the sample,

$(I_e)_{sec}$ is the secondary emission current from the sample surface,

$(I_e)_{BS}$ is the backscattered current from the sample surface,

$(I_e)_{cond}$ is the current conducted through the sample,

$(I_e)_{stored}$ is the transient current stored in the sample,

$(I_e)_{ty}$ is the sum of the secondary of backscatter currents,

ϵ_R is the total yield of surface (secondary and backscatter yields),

ΔV is the voltage across the sample,

R is the resistance through the sample,

C is the sample capacitance, and

t is the time.

If the incident current as a function of time were known, then it would be possible to compute the total yield coefficient for comparison to other data. However, complications arise when considering charging of dielectrics. As dielectrics are charged by monoenergetic electron beams, the electron energy of the impinging particles (i.e., the difference between the beam energy and the surface voltage) changes. In addition, the beam is spread so that electrons strike the region away from the center at various angles, causing the pronounced edge voltage distributions observed in the surface voltage profiles. A sophisticated computer program is required to treat this problem accurately.

However, a value for the total yield can be approximated by making simplifying assumptions. First, we consider only equilibrium conditions to eliminate the stored-current term. Next we consider only that small area in the nominal center of

the sample which will not have electron-beam spreading (all electrons will be assumed to have normal incidence here). Finally, cylindrical-probe theory[20] is assumed valid to compute the equilibrium-current density from the initial-current density. This last assumption has been used to successfully model the charging behavior of Teflon.[21] The resulting equations are

$$(j_e)_{in} = \epsilon_R (j_e)_{in} + \frac{\sigma \Delta V}{d} \quad ,$$

where area is cancelled out, resistance is converted to a conductivity term, and current density replaces the incident current;

$$\epsilon_R = 1 - \frac{\sigma |V_s|}{|j_e| d},$$

and

$$j_e = j_{eo} \frac{V_B - V_s}{V_B} \quad ,$$

where

j_{eo}	is the initial electron current density,
$j_{e;}\|_{initial}$	(The initial electron current density is inferred from measurements by a technique described earlier).
V_B	is the beam voltage,
V_s	is the maximum measured surface voltage for each test, and
σ	is the actual conductivity obtained in each test.

All information needed to evaluate the total yield is available from the experiment. The resulting yields are summarized in Table 1.

The yield data obtained by this technique covers only a limited region of the overall curve. The results can be compared to the data that NASCAP uses[17] and to results obtained on the total yield of Kapton obtained at Case-Western Reserve University.[13] This comparison is given in Figure 32. It is interesting to note that there is a discrepancy between the two yield curves. The maximum yield is different and the second cross-over for unity yield is about 200 V apart. The data obtained in these tests tend to favor the NASCAP curve. The total yield data are important for predicting behavior in charged-particle environments, and the discrepancy should be resolved.

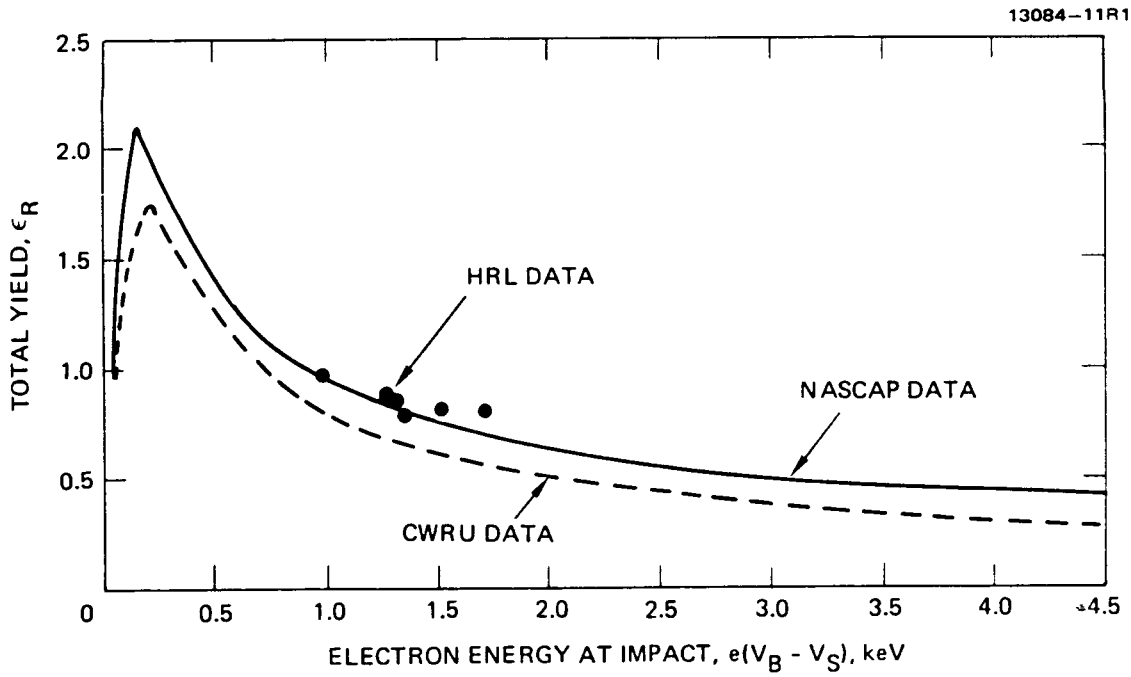

Figure 32. Total yield as function of impact energy Kapton sample.

SECTION 3

ANALYTICAL INVESTIGATION

3.1 NASCAP MODELING

3.1.1 Overview

The NASA Charging Analyzer Program (NASCAP) computer code was developed specifically for the AF/NASA Spacecraft Charging Investigation to predict the response of 3-dimensional objects to environmental fluxes. The code flowchart is shown in Figure 33.

This code has been described in the literature and its capabilities will only be summarized here.[8-10] NASCAP is a quasi-static computational code; that is, it assumes that currents are functions of environmental parameters, electrostatic potentials and magnetostatic fields. It is capable of analyzing the charging behavior of arbitrarily shaped objects covered with various materials as a function of time of exposure to environmental fluxes. It can accept either a space-environment definition or ground-simulation fluxes.

The object must be defined within an inner grid of 17x17x33 points. Furthermore, the object must be described by rectangular parallelipipeds or sections of parallellipipeds; curved surfaces are not allowed. To minimize computer storage and to speed computations, the code uses a system of nested grids, i.e., the 17x17x33 point grid surrounding the inner grid has dimensions twice as big as the inner grid, and so forth. This means that the farther away the object, the coarser the gridding.

For the study conducted here, the ground-simulation mode of code operation was used. The version of the code used required that the tank walls be located properly and grounded. The electron gun must be located at the center of the X-Y mesh and the electrons can only be accelerated in the Z direction. These constraints have been relaxed in more recent versions of the code.

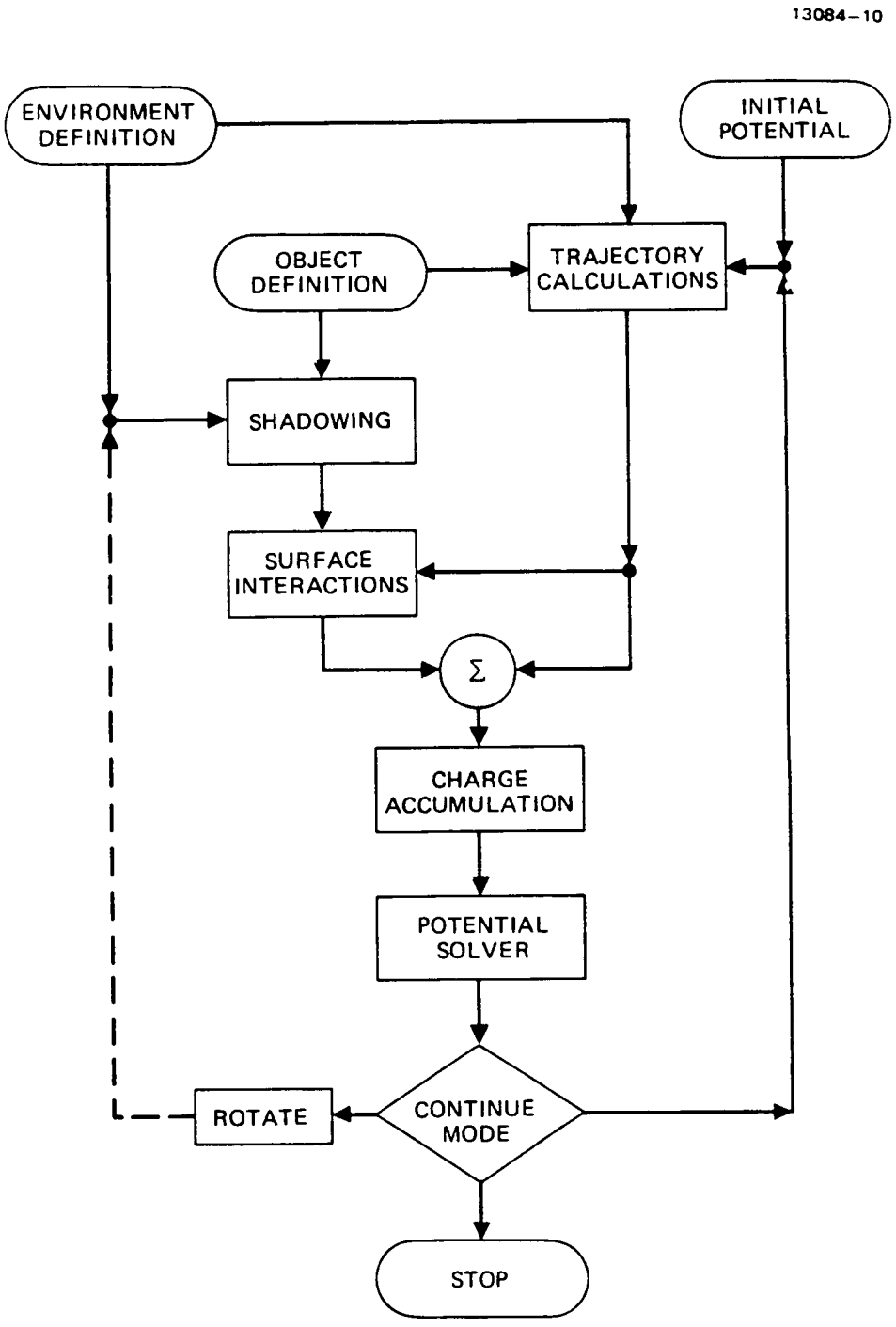

Figure 33. NASCAP flow chart.

The code output includes a variety of graphic and printed data displays. Graphic output includes the material and perspective object definition plots, potential contour plots and particle trajectory plots. The printed output includes a summary of all cell voltages, listing of currents to specified surfaces and compilation of electric fields.

3.1.2 NASCAP Model of Experimental System

Two models of the experimental arrangement were generated, which are illustrated in Figures 34 and 35. The first model included the main chamber walls and located the electron gun at the centerline of the inner grid (see Figure 34). The sample was located at the Z = 27 plane as shown. This model did not attempt to model the sample section chamber (shown in dashed lines) and was used to predict initial voltage profiles and surface voltages using the default material properties (see Table 2).

These initial NASCAP predictions were reviewed to determine what effect the tank walls would have on the voltage profiles. As shown in Figures 36 through 39, the main facility walls do not influence the voltage profiles in space. However, when the smaller chamber walls are drawn in (dashed lines in the figures), then it is obvious that these walls (which are at ground potential) would constrain the voltage build-up in space around the sample and could influence the charging characteristics. The sample area for conducting the tests was reduced from the 0.07 m^2 indicated in the NASCAP runs to the 0.02 m^2 area actually used in the experiments.

The second model was generated at the Lewis Research Center. This model simply located the electron gun and sample within the inner grid and did not attempt to model any walls (see Figure 35). This model used the current Kapton properties (see (Table 2) and was used to evaluate a predicted charging rate for comparison to the experimental value.

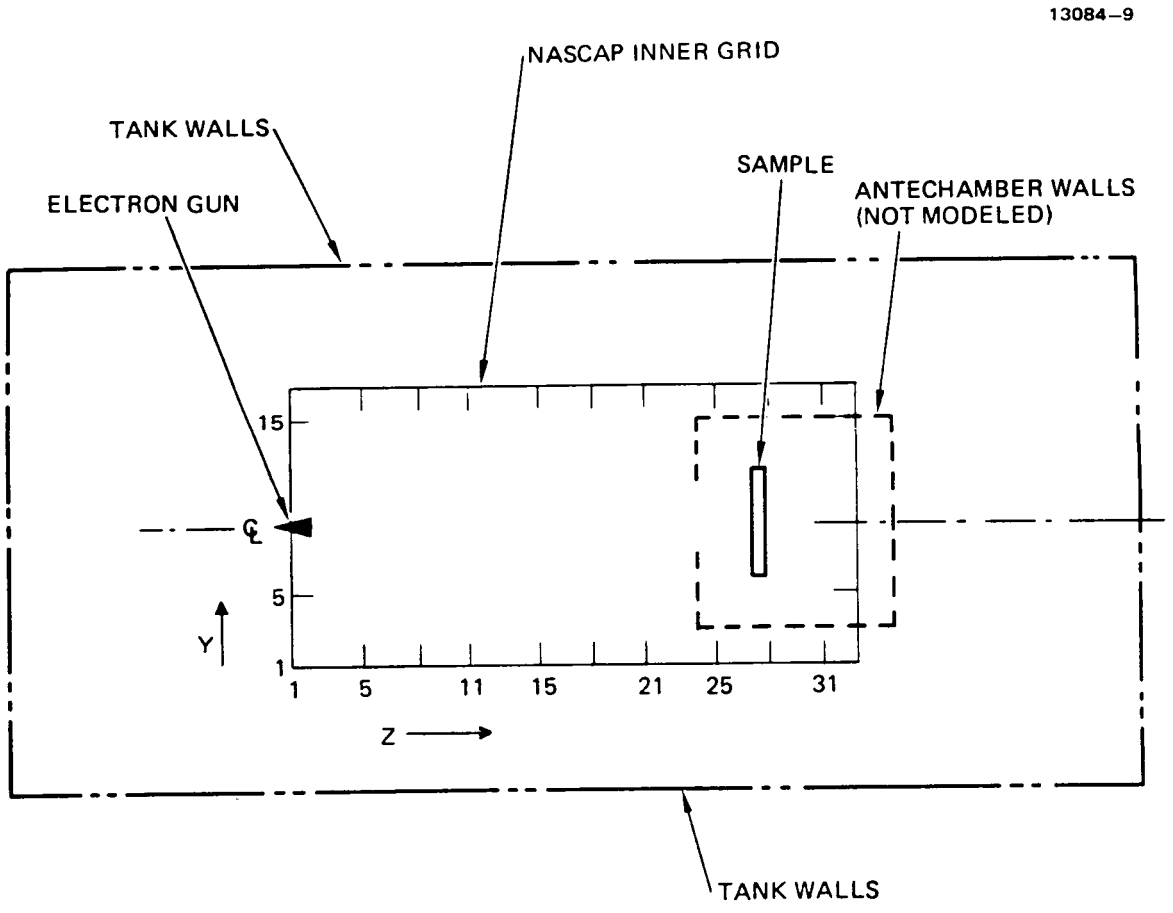

Figure 34. First model used for NASCAP studies.

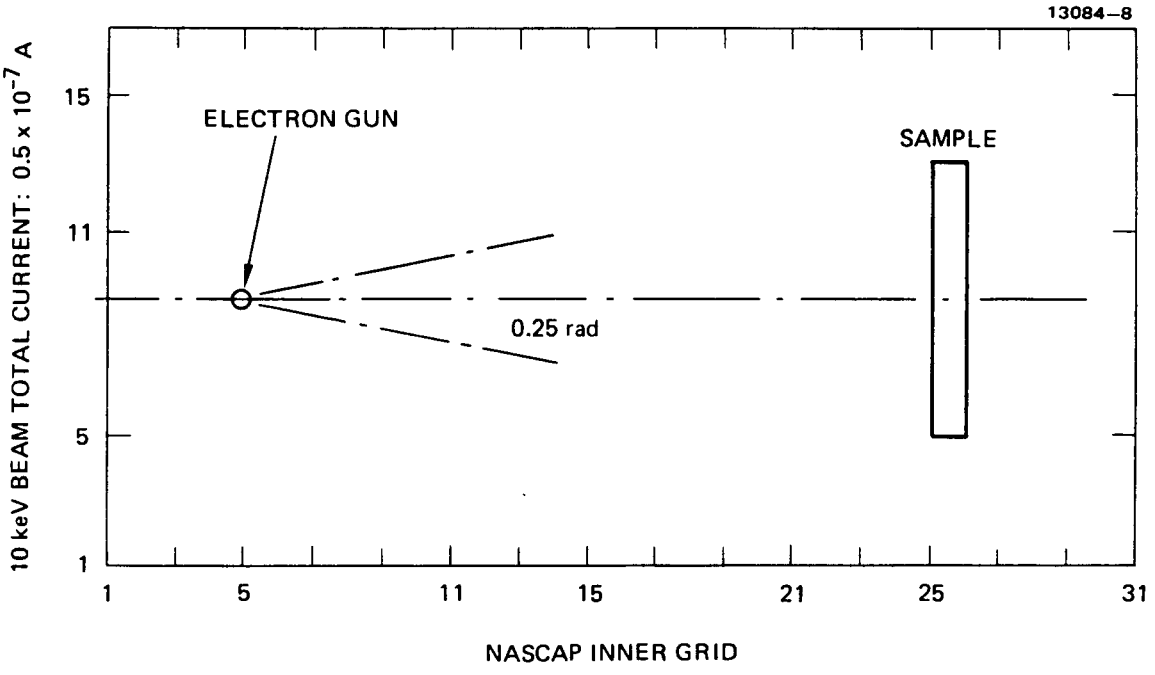

Figure 35. Second model used for NASCAP studies.

TABLE 2. Material Properties Used in NASCAP.

Material Property	Values		
	Model #1	Model #2	Current (As of 2/83)
Dielectric Constant	3.5	3.5	3.0
Thickness (M)	1.27×10^{-4}	1.27×10^{4}	1.27×10^{4}
Bulk Conductivity (S/m)	1×10^{-14}	1×10^{-16}	3×10^{-15}
Atomic Number	5	5	5
Electron Energy for Maximum Yield (keV)	0.150	0.150	0.150
Maximum Secondary Yield	2.1	2.1	2.1
Range (nm) Values Used to Exponent Compute Sec- Range (nm) ondary Yield Exponent Curves for Electrons		7.15 0.6 31.2 1.77	7.15 0.6 31.21 1.77
Secondary Yield for 1-keV Protons	1.4	0.455	0.455
Maximum dE/dx for Protons (keV/m)	70	140	140
Photoemission Current Density (A/m^2)	2×10^{-5}	2×10^{-5}	2×10^{-5}
Surface Resistivity (Ω)	1×10^{16}	1×10^{16}	2.5to7.5×10^{12}

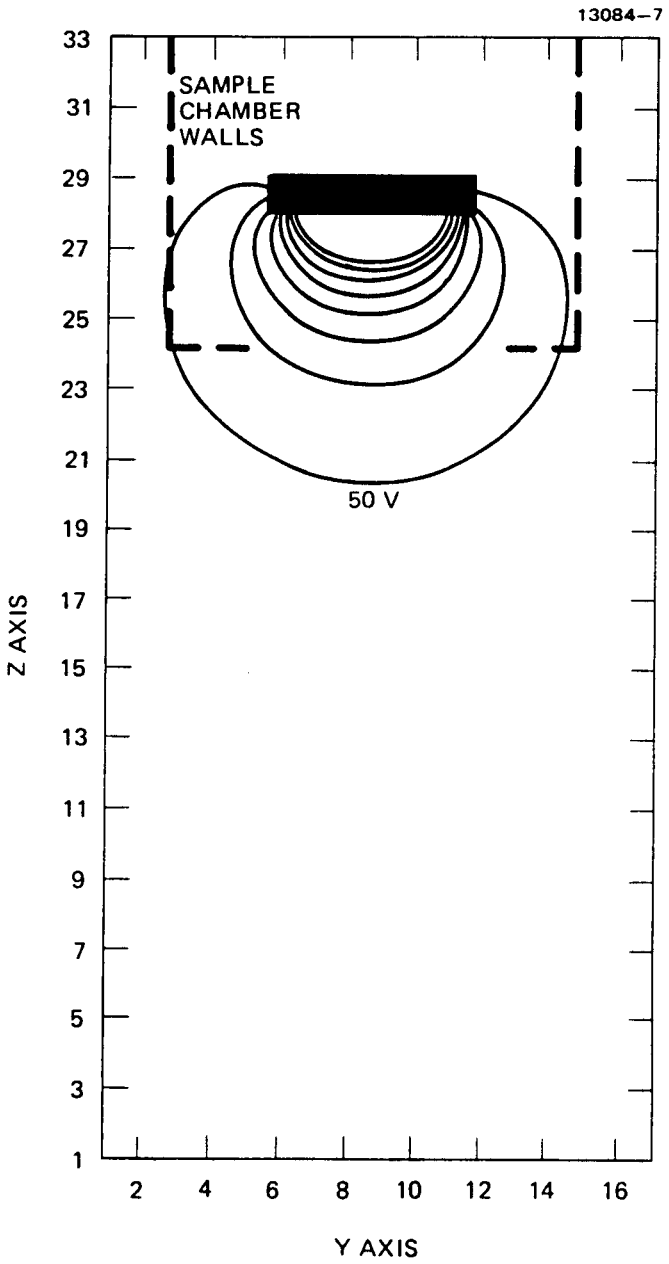

Figure 36. Predicted voltage profiles, showing influence of chamber walls. V_g = 2 kV. Beam Energy = 2 keV Voltage Steps = 50 V

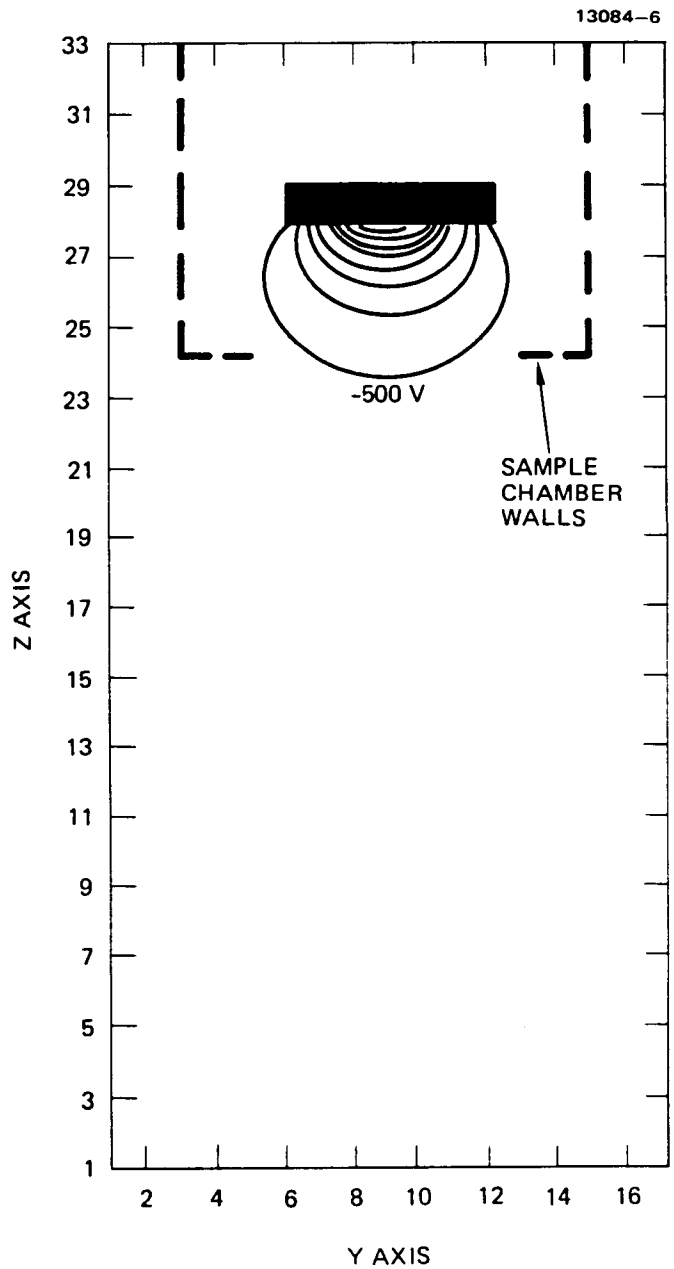

Figure 37. Predicted voltage profiles, showing influence of chamber walls. V_B = 6 kV. Beam Energy = 6 keV Voltage Steps = 500 V

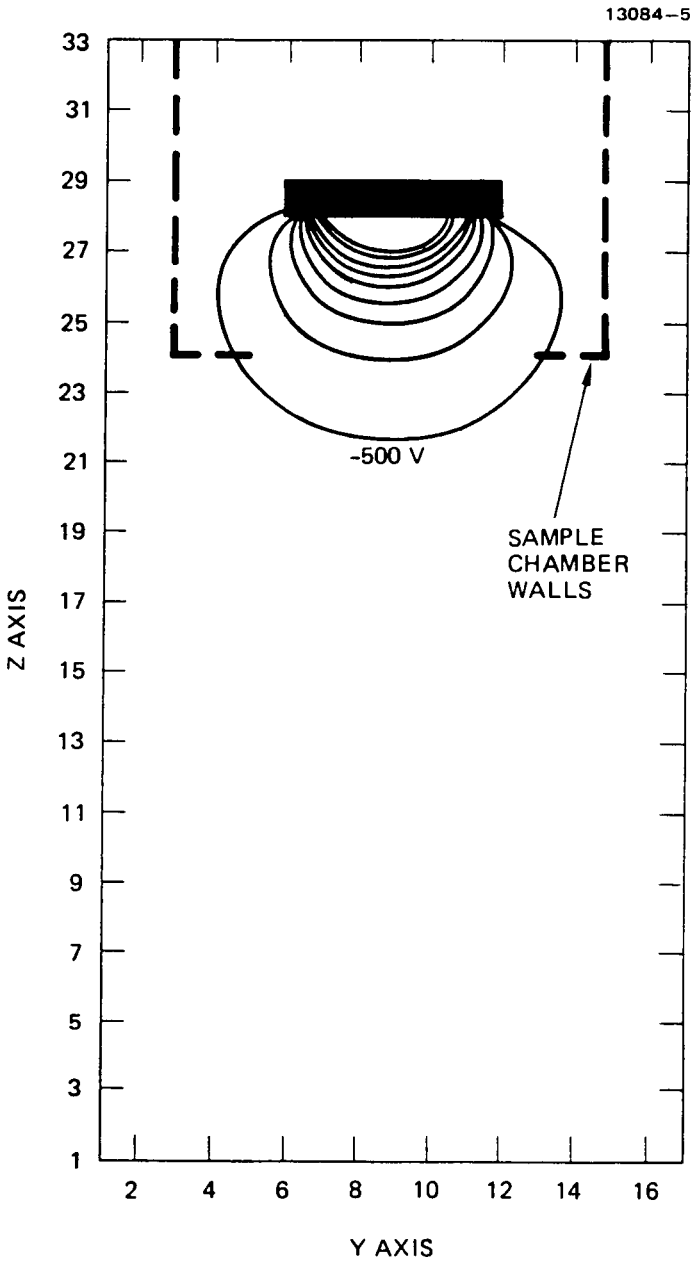

Figure 38. Predicted voltage profiles, showing influence of chamber walls. V_B = 10 kV. Beam Energy = 10 keV Voltage Steps = 500 V.

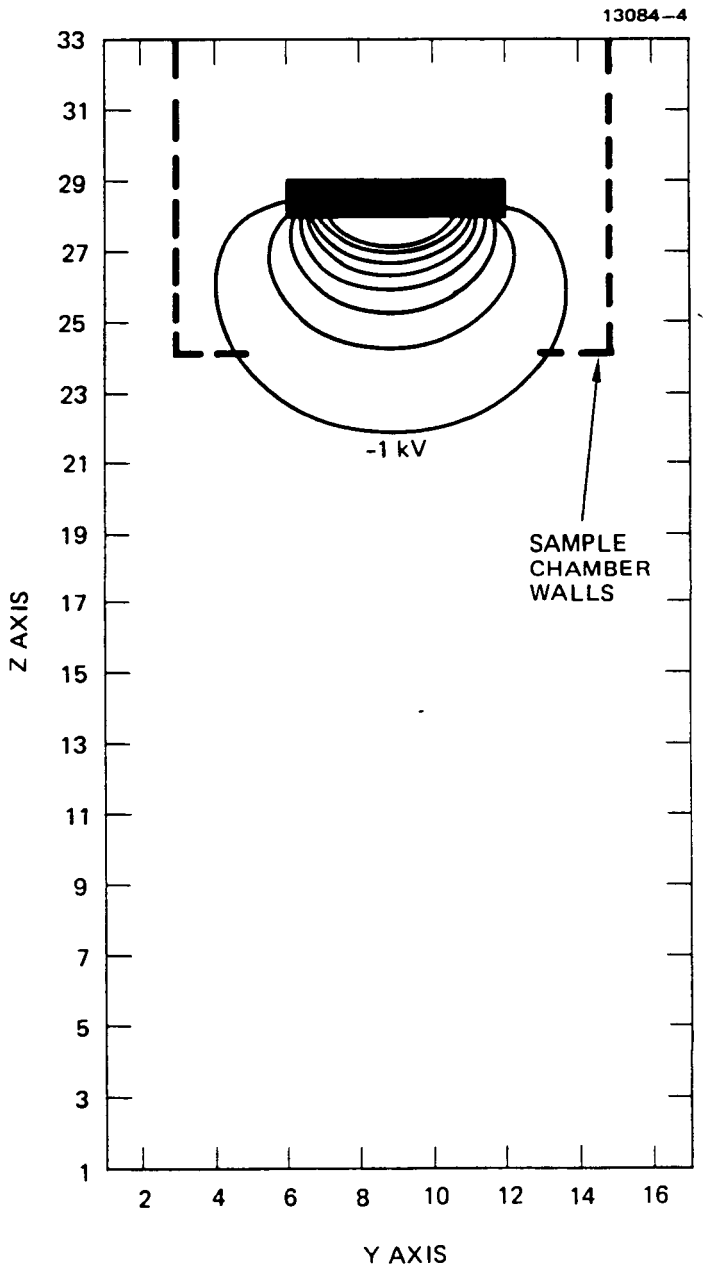

Figure 39. Predicted voltage profiles, showing influence of chamber walls. V_B = 14 kV. Beam Energy = 14 keV Voltage Steps = 1 kV.

3.1.3 Comparison Between NASCAP Predictions and Experimental Data

With the experimentally obtained material parameters in such good agreement with those used by NASCAP, it was anticipated that the predictions should agree very well with the data. When a comparison between the measured and predicted equilibrium voltages is made, the agreement is indeed very good (see Table 3). When the predicted surface-voltage profile is compared with experimental data, the agreement is also excellent (see Figure 40). NASCAP has a finite grid resolution which produces the voltage steps shown.

However, the transient data predictions do not agree with the experimental charging rate data. With the first model, the NASCAP runs were made with an initial current density set at the center of the sample of 11 $\mu A/m^2$. This produced a very rapid predicted charging rate. As a matter of fact, the predicted charging rate for the 2-keV beam conditions was faster than that obtained experimentally for the 15-$\mu A/m^2$ current density data (Figure 41). The second model computer run was made specifically to look at this charging rate question. This run used an initial current density of 2.2 $\mu A/m^2$ and still predicted charging rates faster than the experimental data (see Figure 41). If it is assumed that the experimentally measured data were obtained with an initial current density that was a factor of 3.5 too high, and that the data shifted in time (as was done to data shown in Figure 15), then there is much better agreement between data and predictions. This suggested that a further look at the initial current density would be appropriate.

3.2 EVALUATION OF INITIAL EXPERIMENTAL CURRENT DENSITY

The evaluation of the experimental initial current density was conducted by considering again only the behavior at the center of the sample. This avoided having to deal with beam spreading. The concept used here was to use the first four

Table 3. Comparison of Equilibrium Experimental Surface Voltages to NASCAP Predictions.

Beam Voltage, kV	Surface Voltages (Measured), V	Surface Voltages (Predicted), V	Difference, %
1	-18	0	-
2	-745	-882	18.4
6	-4672	-4750	1.7
10	-8430	-8600	2.0
14	-11,430	-12,400	8.5

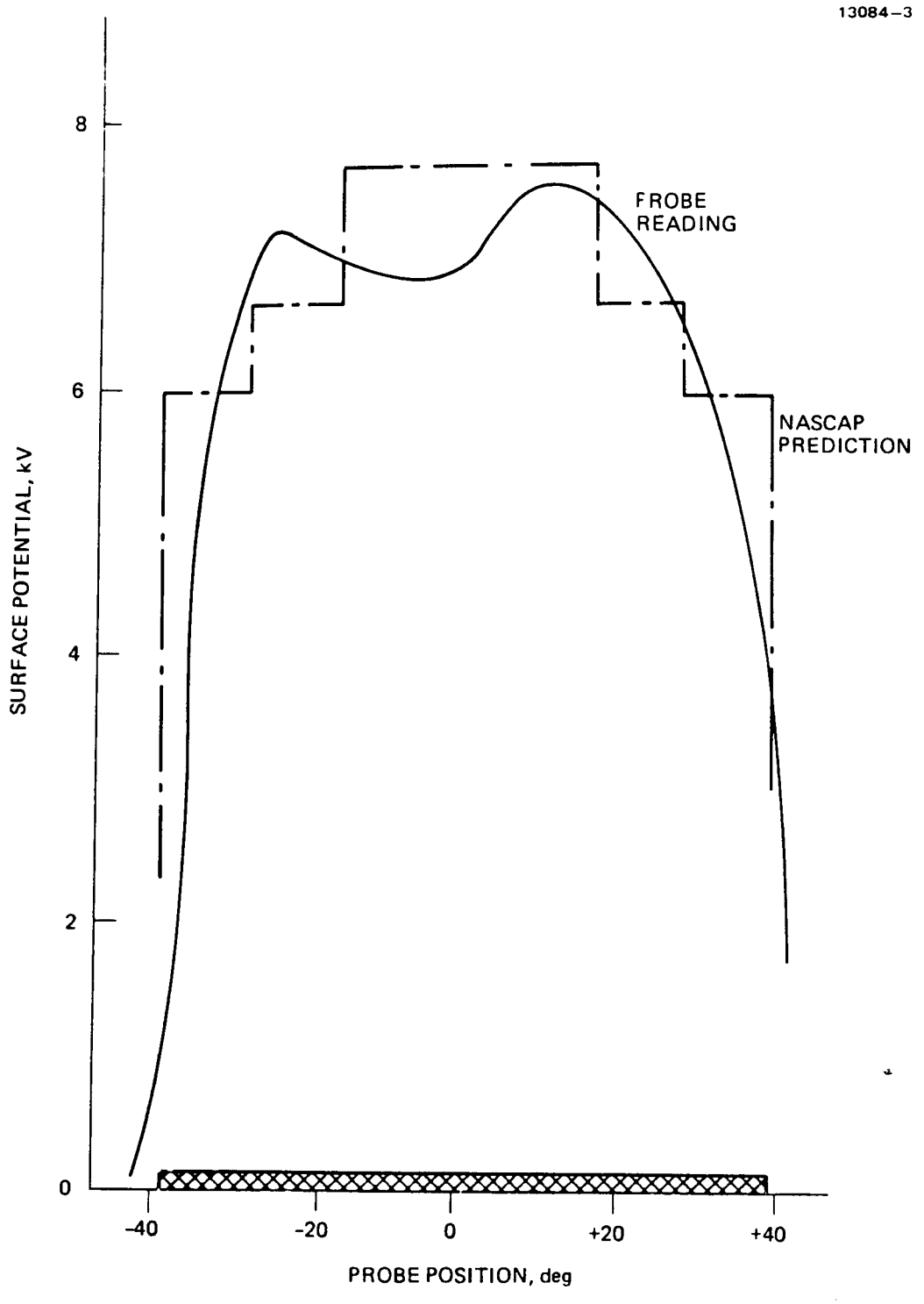

Figure 40. Comparison between voltage profile and NASCAP prediction. (10-keV beam)

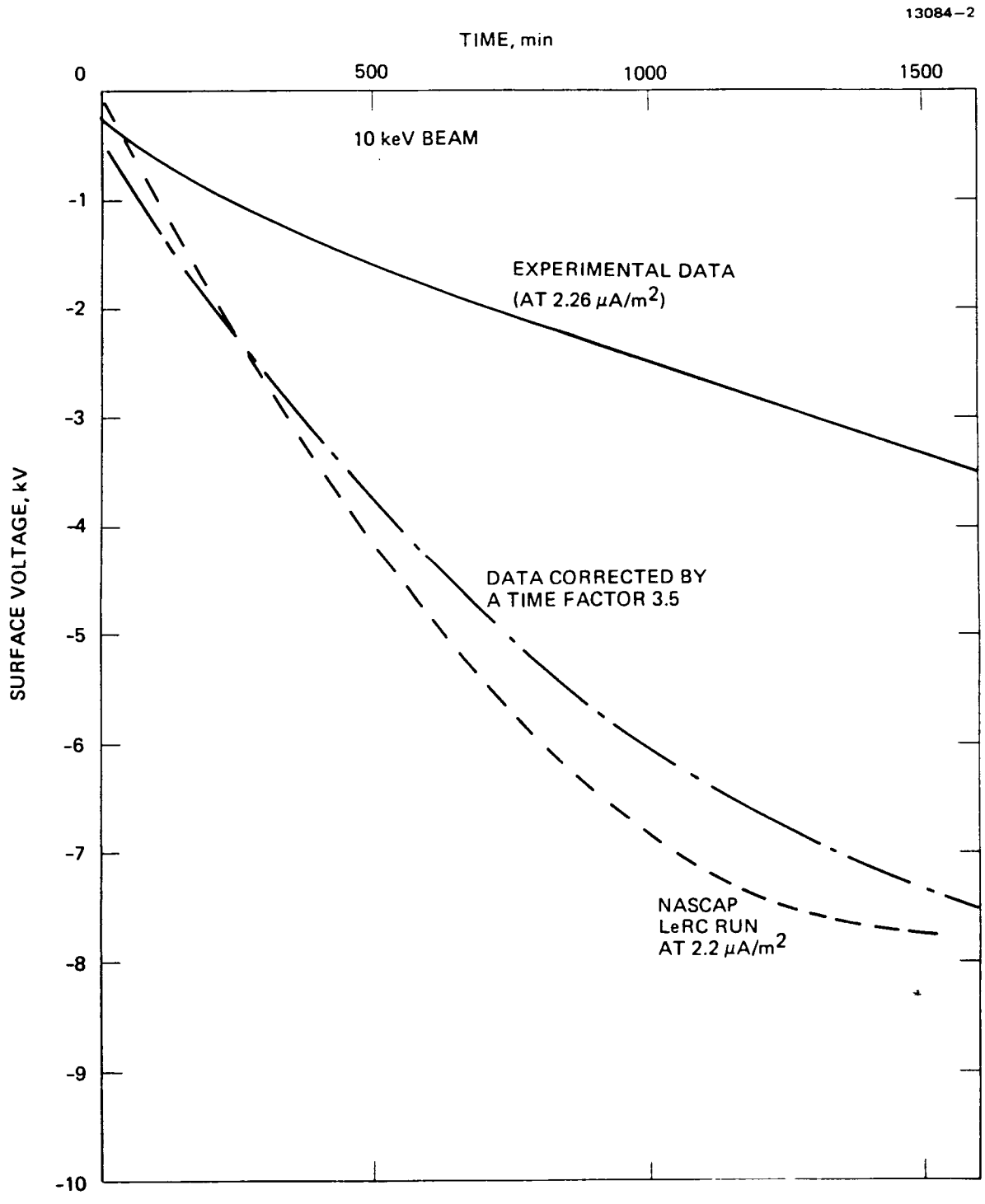

Figure 41. Comparison of experimental data with NASCAP computer run.

surface-voltage data to compute an incident current density at each point and then attempt to extrapolate back to zero time to obtain an indication of an initial current density. The basic relationship used was

$$j_e = \epsilon_R j_e + \frac{\sigma V_{s1}}{d} + \frac{C}{A}\frac{dV}{dt}$$

or

$$j_e = \frac{1}{1 - \epsilon_R}\frac{\sigma V_{s1}}{d} + \frac{\kappa E_o}{d}\frac{\Delta V}{\Delta t} \quad .$$

where ϵ_R is the total yield coefficient (function of $V_B - V_{s1}$), σ is the experimentally obtained conductivity (S/m), Δt is the time interval considered, ΔV is the voltage difference in that time interval t, d is the sample thickness (1.27×10^{-4} m), κ is the dielectric constant (3.5), and ϵ_o is a constant (8.85×10^{-12} F/m). The value for the total yield as a function of impact energy was obtained from the NASCAP total yield data. The results of this computation for the 4-, 8-, 10- and 12-keV beam conditions is tabulated in Table 4 and plotted in Figure 42.

The results shown in Figure 42 are quite interesting in that there appears to be two different types of behavior. In the 4- and 8-keV beam tests, voltage sweeps were not taken until the test was underway for about 110 s. These data indicate that the effective initial electron current density would be about 0.7 $\mu A/m^2$ instead of the value of about 3 $\mu A/m^2$ originally reported from the Faraday cup measurements at the start of each test. Subsequent experimental measurements confirmed that the probe measurements were in fact erroneous by the value indicated.

The 10- and 12-keV beam data had surface-voltage probe sweeps initiated within the first half-minute after the test started. These data show that, while the initial setting could be high within the first minute of operation, the current density

TABLE 4. Data Used to Compute Initial Current Density.

	Time		Surface Voltages						
Beam Energy keV	Interval, s	ΔT, s	Final, V	Initial, V	Average, V	ΔV, V	$V_B - V_S$, V	ϵ_R	j_e, $\mu A/m^2$
4	0-108	108	-170	0	-85	-170	3915	0.42	0.670
	108-180	72	-274	-170	-222	-104	3778	0.43	0.638
	180-324	144	-449	-274	-361.5	-175	3638.5	0.44	0.563
	324-540	216	-669	-449	-559	-220	3441	0.46	0.514
8	0-108	108	-449	-248	-348.5	-201	7651.5	0.28	0.646
	108-287.4	179.4	-771	-449	-610	-322	7390	0.285	0.639
	287.4-611.6	324.2	-1153	-771	-962	-382	7038	0.30	0.473
	611.6-827.6	216	-1511	-1153	-1332	-358	6668	0.305	0.642
10	0-36	36	-694	-200	-447	-494	9553	0.255	4.50
	36-180	144	-999	-694	-846.5	-305	9153.5	0.26	0.72
	180-324.6	144.6	-325	-999	-1162	-326	8838	0.265	0.778
	324.6-504.6	180	-1680	-1325	-1502.5	-355	8497.5	0.27	0.698
	504.6-864.6	360	-2367	-1680	-2023.5	-687	7976.5	0.28	0.70
12	0-36.6	36.6	-1154	-180	-667	-974	11,333	0.22	8.34
	36.6-144	107.4	-1442	-1154	-1298	-288	10,702	0.235	0.866
	144-288	144	-1779	-1442	-1610.5	-337	10,389.5	0.24	0.791
	288-432	144	-2072	-1779	-1925.5	-293	10,074.5	0.245	0.705
	432-864	432	-3178	-2072	-262.5	-1106	9,375	0.255	0.905

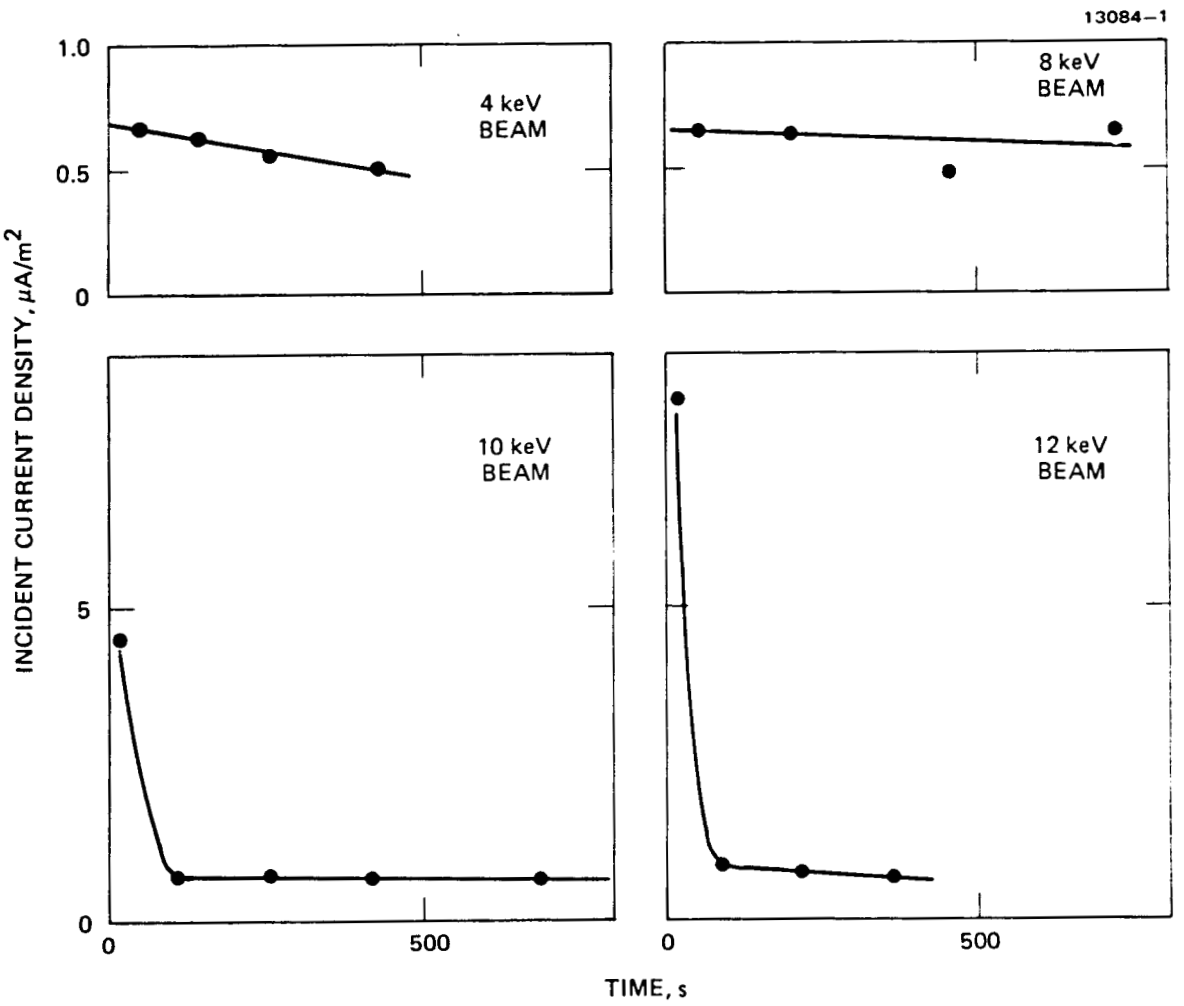

Figure 42. Computed initial incident current density.

fell off to a value of ~0.7 $\mu A/m^2$. The reason for this behavior is not known. It could be due to the charging of some material in the chamber, or to operator error. Whatever the reason, at the very low current densities indicated, the predicted charging rates – shifted to account for the changed incident current density – agree with the experimental results (see Figure 41).

SECTION 4

SUMMARY AND RECOMMENDATIONS

An investigation has been conducted to make measurements of the effective charging properties of Kapton samples exposed to various environmental fluxes. The goal of this investigation was to compare these properties with those used by the NASA Charging Analyzer Program (NASCAP) and suggest whether changes are required. In this study, a 5-mil aluminized Kapton sample, with edges wrapped around the grounded substrate, was evaluated when exposed to a monoenergetic electron beam at 1-kV, 2-kV, 4-kV, 6-kV, 10-kV, 12-kV, and 14-kV accelerator potentials. All tests were run with normal electron incidence and at a few $\mu A/cm^2$ current densities. The experimental results have been compared to NASCAP predictions.

In the experimental investigation the low electron current densities produced very long charging times – hours to reach equilibrium. Test durations of these lengths of time have not been used in the past. The results of such low current density tests are:

- The transition from emission-dominated charging to leakage-dominated charging is apparent at beam voltages above 8 keV. This condition arises when the leakage current becomes an appreciable fraction of the incident electron current.
- Discharges occurred at low beam energies.

The surface-voltage characteristics obtained agreed with expectations. The charging to equilibrium took progressively longer times as the beam voltages were increased, and the profiles across the sample showed the uniform potential in the center region with characteristic fall-off at the edges.

A value for the effective conductivity and dielectric constant and estimates of the total yield over a limited impact energy range can be obtained from the experimental data for

comparison to properties used by NASCAP. The average value obtained for the effective conductivity was 5.7×10^{-15} S/m. It should be compared to the 3×10^{-15} S/m bulk conductivity value used by NASCAP. The apparent trend obtained in the experiment in which the conductivity decreased with increasing voltage gradients is not as expected from the literature on Kapton, and other experimental results and should be evaluated further.

The dielectric constant was obtained from the experimental data by integrating the transient leakage current curve to obtain the charge stored and by computing the constant, assuming a parallel-plate-capacitor relationship. The average value obtained was $\kappa_{exp} = 3.5$ which should be compared to the literature value of $\kappa = 3.5$ and the NASCAP value of $\kappa = 3.0$. This agreement is reasonable considering the approximations that were made to flare a curve through the leakage current data which was responding to discharges.

The total yield was calculated from equilibrium data for impact energies between 0.98 kV $< |V_B - V_S| <$ 1.70 kV. The yields obtained agreed with the NASCAP data in preference to the data obtained by Case Western Reserve University tests. The discrepancy between these sets of data should be evaluated.

The NASCAP computer simulations obtained as part of this study generated predictions that agreed with the equilibrium surface voltages and the surface voltage profiles. However, there were significant deviations between the predicted and actual charging rates. This is surprising considering the reasonable agreement obtained for the dielectric constant and total yields (i.e., those properties that should control charging rates). The deviation between the rates is about a factor of four. Subsequent experimental investigation has shown that this error resulted from improper installation of the Faraday-cup probe.

REFERENCES

1. D.A. McPherson and W.R. Schober, "Spacecraft Charging at High Altitudes: The SCATHA Satellite Program," in Spacecraft Charging by Magnetospheric Plasmas, ed. A. Rosen (Progress in Astronautics and Aeronautics, 47, 15-30, AIAA, N.Y. 1976).

2. R.D. Sharp, E.G. Shelley, and G. Paschmann, "Preliminary Results of a Low Energy Particle Survey at Synchronous Altitude," Jour. Geophys. Res. 75, 6092 (1970).

3. S.E. DeForest and C.E. McIlwain, "Plasma Clouds in the Magnetosphere," Jour. Geophys. Res. 76, 3587-3611 (1971).

4. S.E. DeForest, "Spacecraft Charging at Synchronous Orbits, Jour. Geophys. Res. 76, 651-659 (1972).

5. D.L. Reasoner, W. Lennartsson, and C.R. Chappell, "Relationship Between ATS-6 Spacecraft Occurrences and Warm Plasma Encounters," in Spacecraft Charging by Magnetospheric Plasmas, ed. A. Rosen (Progress in Astronautics and Aeronautics 47, 89-101, 1976).

6. R.C. Olsen, E.C. Whipple, and C.K. Purvis, "Active Modification of ATS-5 and ATS-6 Spacecraft Potentials," in Proceedings of the 1978 Symposium in the Effect of the Ionosphere on Space and Terrestrial Systems, Naval Research Laboratory and Office of Naval Research, Washington, D.C., 24-26 Jan., 1978, Paper 4-9.

7. R.R. Lovell, N.J. Stevens, W.R. Schober, C.P. Pike, and Wm. Lehn, "Spacecraft Charging Investigation: A Joint Research and Technology Program," in Spacecraft Charging by Magnetospheric Plasmas, ed. A. Rosen (Progress in Astronautics and Aeronautics, 47, 3-14, AIAA, N.Y. 1976).

8. I. Katz, J.J. Cassidy, M.J. Mandell, G.W. Schneulle, P.G. Steen, and J.C. Roche, "The Capabilities of the NASA Charging Analyzer Program," Spacecraft Charging Technology - 1978, NASA CP-2071/AFGL-TR-79-0082, 1979, pp. 101-122.

9. A.G. Rubin, I. Katz, M.J. Mandell, G.W. Schneulle, P.G. Steen, D.E. Parks, J.J. Cassidy, and J.L. Roche, "A Three-Dimensional Spacecraft Charging Computer Code," in Space Systems and Their Interactions with Earth's Space Environment, ed. H.B. Garrett and C.P. Pike (Progress in Astronautics and Aeronautics 71, 318-336, 1980).

10. P.R. Stannard, I. Katz, L. Gedeon, J.C. Roche, A.G. Rubin, and M.F. Tautz, "Validation of the NASCAP Model Using Spaceflight Data," AIAA Paper 82-0269, Jan. 1982.

11. N.J. Stevens, F.D. Berkopec, J.V. Staskus, R.A. Blech, and S.J. Narcisco, "Testing of Typical Spacecraft Materials in a Simulated Substorm Environment", Proceedings of the Spacecraft Charging Technology Conference, eds. C.P. Pike and R.R. Lovell, AFGL-TR-77-0051/NASA TMX-73537, Feb. 1977, pp. 431-458.

12. J.V. Staskus and J.C. Roche, "Testing of a Spacecraft Model in a Combined Environment Simulator", IEEE Transactions on Nuclear Science, NS-28, 4509-4512. (1981).

13. I. Krainsky, W. Lundin, W.L. Gordon, and R.W. Hoffman, "Secondary Electron Emission Yield," Annual Report for July 1980 - June 1981, NASA Grant NSG-3197, Case Western Reserve University, Sept. 1981.

14. C.K. Purvis and J.V. Staskus, "SCATHA SSPM Charging Response; NASCAP Predictions Compared to Data" in Spacecraft Charging Technology - 1980, NASA CP-2182/AFGL-TR-81-0270, 1981, pp. 592-607.

15. P.A. Robinson, E.M. Brown, S.M. Conan, C.R. Dulgeroff, W.R. Elkman, G.L. Holm, L.C. Lawton, G.J. Pack, and D.L. Shannon, "Evaluation of Charge Control Techniques on Spacecraft Thermal Surfaces (Electrostatic Discharge Study)" in Spacecraft Charging Technology - 1980, NASA CP-2182/AFGL-TR-81-0270, 1981, pp. 320-341.

16. H.T. Coffey, J.E. Nanevicz, and R.C. Adams, "Photoconductivity of High-Voltage Space Insulating Materials," NASA CR-134995, Oct. 1975.

17. C.K. Purvis, Kapton Total Yield Data from NASCAP, private communications.

18. C.K. Purvis, "Status of Materials Characterization Studies," Spacecraft Charging Technology - 1978, NASA CP-2071/AFGL-TR-79-0082, 1979, pp. 437-456.

19. C.K. Purvis, "Evolution of Spacecraft Charging Technology," AIAA Paper 82-0273 (1982).

20. F.F Chen, "Electric Probes," Pure and Applied Physics 21, Plasma Diagnostic Techniques, eds. R.H. Huddlestone and S.L. Leonard (Academic Press, 1965), pp. 113-119.

21. C.K. Purvis, N.J. Stevens, and J.C. Olgebay, "Charging Characteristics of Materials: Comparison of Experimental Results with Simple Analytical Models," in Proceedings of the Spacecraft Charging Technology Conference, eds. C.P. Pike and R.R. Lovell, AFGL-TR-0051/NASA TMX-73537, Feb. 1977, pp. 459-486.

Daniel Hastings
Mass. Inst. of Technology
Dept. of Aeronautics & Astronautics
Cambridge, MA 02139

Robert C. Hazelton
Inland Motor Research
Development Center
801 First Street
Radford, VA 24141

Calvin Herman
EH-431
NASA Johnson Space Center
Houston, TX 77058

O. L. Husmann
MBB Space West Division
D-8000 Munich 80
Munich, West Germany

Dr. Gary A. Jongeward
S-CUBED, Div. of Maxwell Labs
3398 Carmel Mountain Road
San Diego, CA 92121-1095

Dr. Ira Katz
S-CUBED, Div. of Maxwell Labs
3398 Carmel Mountain Road
San Diego, CA 92121-1095

Dr. Bruce Kendall
Pennsylvania State University
104 Davey Lab
University Park, PA 16802

Irwin Krinsky
Univ. of Calif. at San Diego
UCSD C-111
La Jolla, CA 92093

J. C. Laframboise
York University Physics Dept.
4700 Keele St.
Toronto, Ontario, Canada M3J1P3

H. Lechte
Hd., Spacecraft Sys.
ESA/ESTEC
Keplerlaan 1
2201 AZ Noordwijk
THE NETHERLANDS

Phillip L. Leung, MS-144-218
NASA Jet Propulsion Laboratory
4800 Oak Grove Drive
Pasadena, CA 91109

Dr. Harold Liemohn
Boeing Aerospace Co.
P.O. Box 3999, MS BC-23
Seattle, WA 98124

R. Lopez
Rice University
Dept. of Space Physics & Astronmy
Houston, TX 77251

Derek Mahaffey
Boeing Aerospace Co.
P.O. Box 3999, MS 87-60
Seattle, WA 98124-2499

Dr. Myron J. Mandell
S-CUBED, Div. of Maxwell Labs
3398 Carmel Mountain Road
San Diego, CA 92121-1095

Andrew Meulenberg
COMSAT Lab.
22300 Comsat Dr.
Clarksburg, MD 20871

Richard C. Adamo
SRI International
333 Ravenswood Ave.
Menlo Park, CA 94025

Prof. Thomas P. Armstrong
Dept. of Physics
University of Kansas
Lawrence, KS 66045

Keith G. Balmain
Dept. of Electrical Engineering
University of Toronto
Toronto, Ontario, Canada M5S1A4

Brian L. Beers
Beers Associates, Inc.
11495 Commerce Park Drive
Reston, VA 22091

Renate Bever
Code 711.3
NASA Goddard Space Flight Ctr.
Greenbelt, MD 10771

K. P. Bogus
Head, Solar Generators Section
ESA/ESTEC
Keplerlaan 1
2201 AZ Noordwijk
THE NETHERLANDS

William J. Burke
AFGL/PHG
Hanscom AFB, MA 01731

Ralph Carruth
NASA Marshal Space Flight Ctr.
Mail Code EH-12
Huntsville, AL 35812

Dr. Peter Coakley
JAYCOR
P.O. Box 85154
San Diego, CA 92133

Hebert A. Cohen
WJ Schafer Associates
1901 N. Ft Myer Drive, Suite 800
Arlington, VA 22209

David B. Cotts
Polymer Science Dept.
SRI International
333 Ravenswood Ave.
Menlo Park, CA 94025

Delia E. Donatelli
AFGL/PHG
Hanscom AFB, MA 01731

A. Robb Frederickson
ESD/ESR/RADC
Hanscom AFB, MA 01731

Dr. Henry B. Garrett MS 301-456
NASA Jet Propulsion Laboratory
4800 Oak Grove Drive
Pasadena, CA 91109

William L. Gordon
Dept. of Physics
Case Western Reserve University
Cleveland, OH 44106

William N. Hall
AFGL/PHK
Hanscom AFB, MA 01731

Joseph Nanevicz
SRI International
333 Ravenswood Ave.
Menlo Park, CA 94025

Alain Paillous
Centre d'Etude et de Recher
ches de Toulouse
B.P. 4025
Toulouse, CEDEX, France 31005

Lee Parker
Lee W. Parker, Inc.
252 Lexington Rd.
Concord, MA 01742

Charles P. Pike
AFGL/PHK
Hanscom AFB, MA 01731

Gregory M. Plamp
JAYCOR
150 E. Highland Ave. Apt E
Sierra Madre, CA 91024

Carolyn K. Purvis MS 302-1
NASA Lewis Research Center
21000 Brookpark Road
Cleveland, OH 44135

John Reddy
European Space Agency/ESTEC
TTM
Noordwijk,
THE NETHERLANDS

Bertram Shuman
AFGL/PHK
Hanscom AFB, MA 01731

(25 copies to)
John Staskus MS 302-1
NASA Lewis Research Center
21000 Brookpark Road
Cleveland, OH 44135

N. John Stevens
TRW Space & Technology Group
Mail Stop 135/3266
One Space Park
Redondo Beach, CA 90278

Prof. William B. Thompson
Univ. of Calif. at San Diego
Dept. B-019
La Jolla, CA 92093

Alfred L. Vampola
The Aerospace Corp.
P.O. Box 92957
Los Angeles, CA 90009

Elden C. Whipple
Ctr for Astrophysics & Space Science
Univ. of Calif. at San Diego
La Jolla, CA 92093

Roger Williamson
Stanford University Star Lab
M/S SEL 4055
Stanford, CA 94305

Weldon S. Williamson
Hughes Research Labs
3011 Malibu Canyon Rd
Malibu, CA 90266

Ed Yadlowsky
HY-Tech Research Corp.
P.O. Box 3422
Radford, VA 24243